JOURNAL OF GEOPHYSICAL RESEARCH, VOL. 113, B12406, doi:10.1029/2008JB005684, 2008

Persistent elastic behavior above a megathrust rupture patch: Nias island, West Sumatra

Richard W. Briggs,[1,2] Kerry Sieh,[1,3] William H. Amidon,[1] John Galetzka,[1] Dudi Prayudi,[4] Imam Suprihanto,[5] Nugraha Sastra,[4] Bambang Suwargadi,[4] Danny Natawidjaja,[4] and Thomas G. Farr[6]

Received 11 March 2008; revised 24 July 2008; accepted 17 September 2008; published 12 December 2008.

[1] We quantify fore-arc deformation using fossil reefs to test the assumption commonly made in seismic cycle models that anelastic deformation of the fore arc is negligible. Elevated coral microatolls, paleoreef flats, and chenier plains show that the Sumatran outer arc island of Nias has experienced a complex pattern of relatively slow long-term uplift and subsidence during the Holocene epoch. This same island rose up to 2.9 m during the M_w 8.7 Sunda megathrust rupture in 2005. The mismatch between the 2005 and Holocene uplift patterns, along with the overall low rates of Holocene deformation, reflects the dominance of elastic strain accumulation and release along this section of the Sunda outer arc high and the relatively subordinate role of upper plate deformation in accommodating long-term plate convergence. The fraction of 2005 uplift that will be retained permanently is generally <4% for sites that experienced more than 0.25 m of coseismic uplift. Average uplift rates since the mid-Holocene range from 1.5 to −0.2 mm/a and are highest on the eastern coast of Nias, where coseismic uplift was nearly zero in 2005. The pattern of long-term uplift and subsidence is consistent with slow deformation of Nias along closely spaced folds in the north and trenchward dipping back thrusts in the southeast. Low Holocene tectonic uplift rates provide for excellent geomorphic and stratigraphic preservation of the mid-Holocene relative sea level high, which was under way by ~7.3 ka and persisted until ~2 ka.

Citation: Briggs, R. W., K. Sieh, W. H. Amidon, J. Galetzka, D. Prayudi, I. Suprihanto, N. Sastra, B. Suwargadi, D. Natawidjaja, and T. G. Farr (2008), Persistent elastic behavior above a megathrust rupture patch: Nias island, West Sumatra, *J. Geophys. Res.*, *113*, B12406, doi:10.1029/2008JB005684.

1. Introduction

[2] Outer-arc islands off the west coast of Sumatra (Figure 1) provide a rare opportunity to compare coseismic to permanent deformation above a megathrust rupture patch. Nias island sits directly above the portion of the Sunda megathrust that slipped as much as 12 m during the March 2005 M_w 8.7 rupture [*Briggs et al.*, 2006; *Konca et al.*, 2007]. The sudden release of accumulated strain caused nearly three meters of uplift on Nias and over a meter of subsidence between the island and the Sumatran mainland, resulting in dramatic coastal changes that will adversely affect human and natural communities in the coming decades (Figure 2).

[3] A comparison of 2005 coseismic to longer-term deformation on Nias is intriguing because it is not yet clear how megathrust slip contributes to permanent vertical deformation of the fore arc. Although it is generally assumed that the fore arc does not accumulate deformation over the long-term [*Savage*, 1983], there are examples where this assumption might not hold. For example, Holocene terraces have clearly accumulated significant long-term uplift in the vicinity of the 1703 Genroku Kanto and 1964 Alaskan events, but these motions most likely reflect movement on faults in the plate above the megathrust [*Plafker*, 1965; *Scholz and Kato*, 1978]. Likewise, net subsidence of tidal estuaries over several Cascadian megathrust rupture cycles along coasts that are otherwise experiencing long-term uplift suggests that intraplate faults dominate the local vertical tectonic signal at short wavelengths and time spans [*Adams*, 1984; *Atwater*, 1987; *Kelsey et al.*, 1994; *McNeill et al.*, 1998].

[4] Elastic dislocation models are particularly successful at reproducing the geodetic pattern of strain accumulation and release associated with the megathrust seismic cycle [*Fitch and Scholz*, 1971; *Savage*, 1983; *Wang et al.*, 2003], but an explicit assumption made in this approach is that anelastic deformation of the fore arc during interseismic or

[1]Tectonics Observatory, Division of Geological and Planetary Sciences, California Institute of Technology, Pasadena, California, USA.
[2]Now at U.S. Geological Survey, Golden, Colorado, USA.
[3]Now at Earth Observatory of Singapore, Singapore.
[4]Research Center for Geotechnology, Indonesian Institute of Sciences, Bandung, Indonesia.
[5]Jakarta, Indonesia.
[6]Jet Propulsion Laboratory, California Institute of Technology, Pasadena, California, USA.

0148-0227/08/2008JB005684$09.00

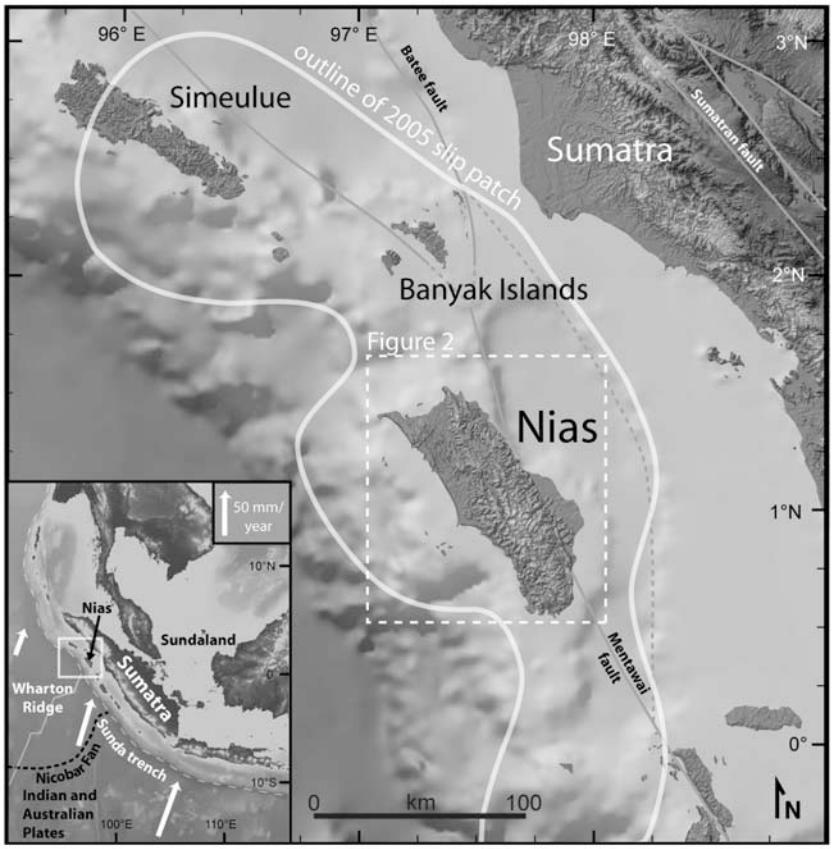

Figure 1. Location of Nias with respect to the 2005 Sunda megathrust rupture patch (outline from *Briggs et al.* [2006]). Convergence vectors between the Indian and Australian plates and the Sunda plate calculated from *Prawirodirdjo and Bock* [2004]. Faults generalized from *Sieh and Natawidjaja* [2000]; bathymetry from *Smith and Sandwell* [1997]; and SRTM topography from http://usgs.seamless.gov.

coseismic deformation can be neglected. Purely elastic behavior implies no net vertical change over a full earthquake cycle, and these models rely on ad hoc corrections to fit observations of permanent uplift or subsidence. The assumption of elastic behavior is clearly a simple approximation that is generally difficult to test since most observations of long-term vertical motion along subduction zones are along the coast and thus distant from megathrust rupture patches. As a consequence, it has been difficult to recognize and analyze permanent uplift and subsidence of the fore arc solely due to megathrust rupture.

[5] It is fortunate that widespread fringing coral reefs, both modern and fossil, occur along the coastal margins of Nias because they allow straightforward comparison of the 2005 coseismic deformation pattern to older, cumulative uplift. Certain species of *Porites* and *Goniastrea* corals form microatolls that function as high-resolution natural tide gauges that are particularly useful for measuring coseismic vertical tectonic motions [*Taylor et al.*, 1987, 1980]. The net tectonic uplift of the corals and their correlative surfaces, when combined with accurate ages, allows us to characterize the style and quantify the rates of crustal deformation [*Chappell*, 1974].

[6] In this paper, we combine geological mapping, stratigraphic and geomorphic analyses, and U-Th and ^{14}C dates on uplifted corals and organic material to determine the pattern of Holocene coastal uplift on Nias. We then contrast the Holocene and 2005 coseismic deformation patterns and discuss the pattern of permanent uplift in the context of the earthquake cycle along this portion of the Sunda megathrust. Our primary goal is to isolate the contribution of megathrust ruptures to upper plate deformation to better understand long-term uplift and subsidence stemming from plate convergence.

2. Tectonic Setting and Geology

[7] At the latitude of Nias, the Indian and Australian plates subduct obliquely beneath Southeast Asia at the rate of 50–70 mm/a [*DeMets et al.*, 1994; *Prawirodirdjo and Bock*, 2004]. Oblique convergence is partitioned into trench-normal contraction accommodated primarily on the Sunda megathrust, and right-lateral shear taken up mainly by the Sumatran fault [*Fitch and Scholz*, 1971] and possibly on the Mentawai fault zone [*Diament et al.*, 1992] (but see *Sieh and Natawidjaja* [2000]). Despite the significant oblique component of convergence, megathrust ruptures such as the 2005 M_w 8.7 and 1861 M_w ~8.4 events [*Newcomb and McCann*, 1987] dominate the historical record of moment release near Nias. A detailed paleoseismic history of the subduction zone in the Nias region does not yet exist, but the nominal recurrence interval between the 1861 and 2005 events is similar to the ~200 years between megathrust ruptures recorded by fossil corals along

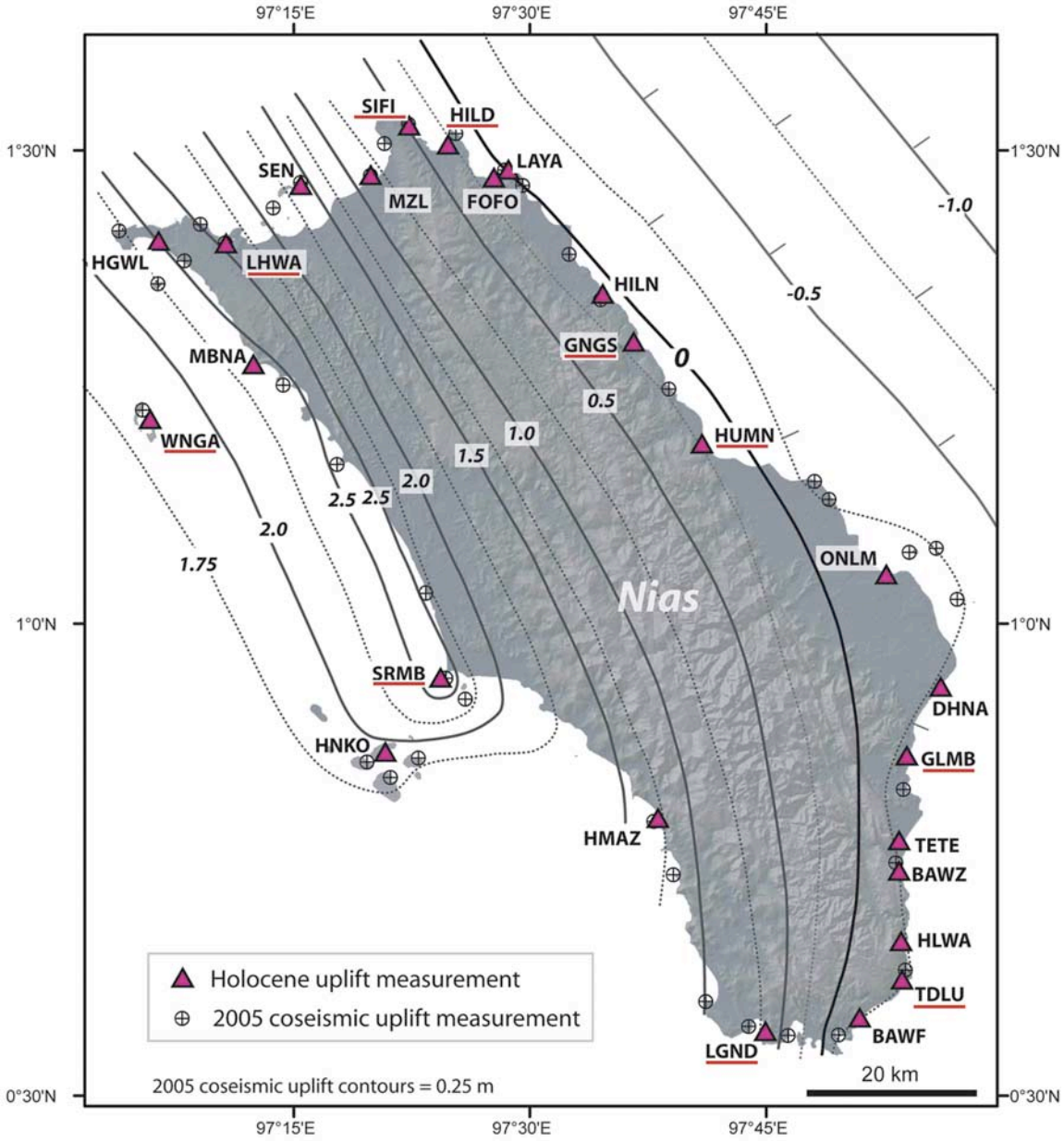

Figure 2. Study sites on Nias with respect to 2005 coseismic uplift values [*Briggs et al.*, 2006]. Sites discussed in the paper are underlined, and the remaining sites are discussed in the auxiliary materials.

the Mentawai islands to the south [*Natawidjaja et al.*, 2007].

[8] Nias is a local high on the prominent outer arc ridge that parallels the Sunda trench for over 2600 km. Subduction along the Sundaland margin was under way by the Late Cretaceous [*Hamilton*, 1979], but the emergence of Nias as an island along the outer arc began in the early Pliocene [*Moore and Karig*, 1980; *Samuel et al.*, 1997]. The island is composed of mid-Oligocene to Pliocene well-bedded abyssal to sublittoral marine sediments and melanges atop pre-Tertiary ophiolitic basement. These older units are faulted and folded and overlain unconformably by relatively undeformed Plio-Pleistocene reef limestones [*Djamal et al.*, 1991; *Samuel et al.*, 1997]. The original depositional environment and the mechanism of subsequent uplift and deformation of thick marine sequences that form the bulk of Nias are subjects of contention [*Barber and Crow*, 2005]. One position [*Moore and Karig*, 1980] holds that the prevailing mode of deformation and uplift has been continual contraction of the accretionary wedge and that accommodation space for the marine sequences was provided by trench slope basins. A contrasting view [*Samuel et al.*, 1997] is that deposition occurred in rift basins atop the Paleogene accretionary complex during periods of pronounced local extension, and that periods of uplift reflect reactivation of extensional faults as thrusts during relatively brief periods of basin inversion. *Hamilton*'s [1979] proposal that the morphology of the outer arc high reflects simultaneous imbrication and gravitational spreading of the accretionary wedge may unite these two interpretations, although

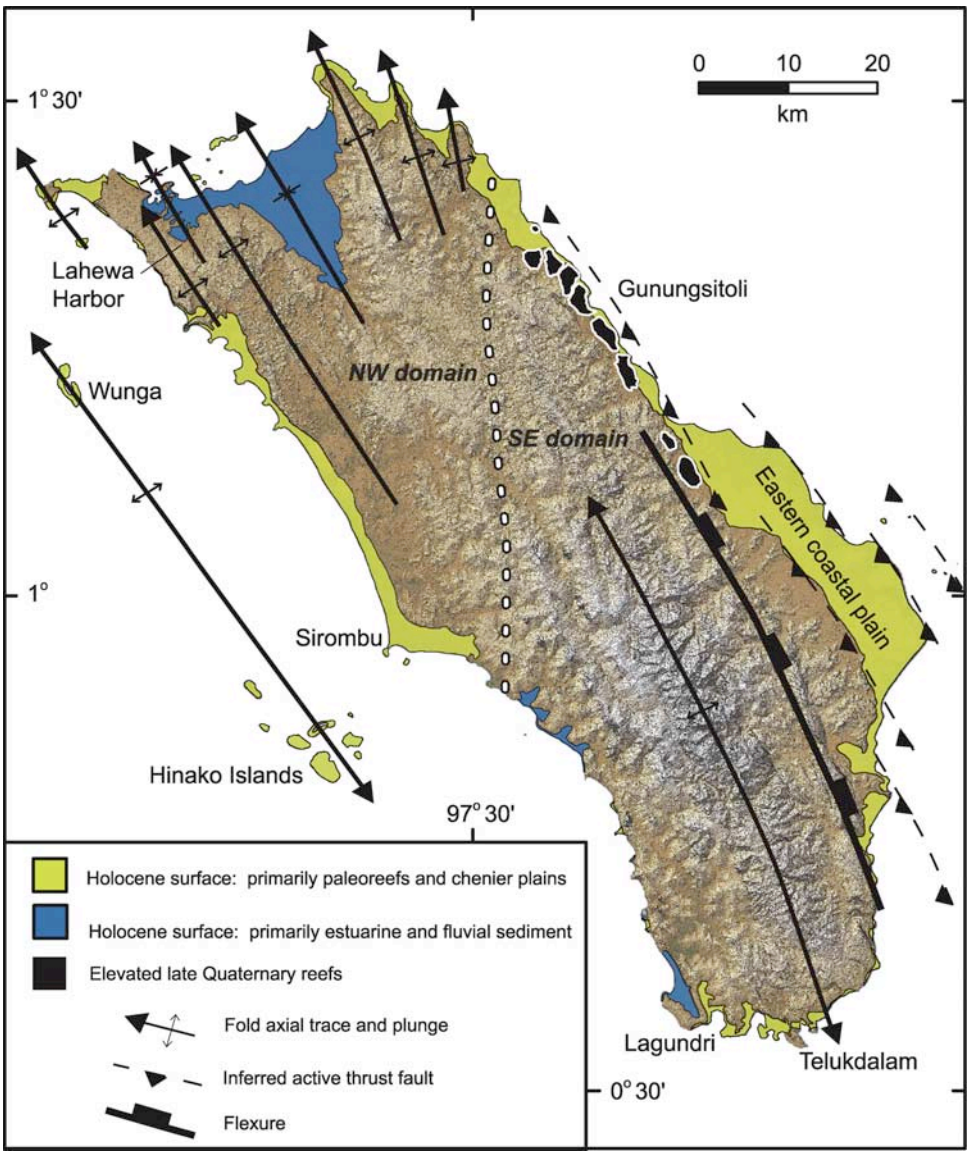

Figure 3. Major active tectonic elements and coastal Holocene surfaces of Nias. Open arrows are fold axes; dashed lines are inferred faults. Dotted white line divides northwest and southeast structural domains. Thick gray line is flexure with blocks on downthrown side. SRTM topography from *Farr et al.* [2007].

the internal mixing of the wedge predicted by Hamilton's model has not been observed in outcrop [*Moore and Karig*, 1980].

[9] Sediment supply to the trench appears to be the primary factor that controls the emergence of islands along the Sunda outer arc high. The average elevation of the Sunda outer arc ridge is clearly correlated with the thickness and extent of the Nicobar Fan [*Curray and Moore*, 1974; *Moore et al.*, 1982], but the mechanisms and structures that control preferential uplift of individual islands are unclear. Pliocene uplift of Nias may have reflected a change in plate convergence direction and rate [*Samuel et al.*, 1997], but presumably this would have affected the entire outer arc high in a similar fashion. Subduction of the fossil Wharton Ridge has been proposed as a cause of focused, episodic extension and contraction in the upper plate along the Sunda arc [*Whittaker et al.*, 2007] that may have influenced uplift of Nias. Recent high-resolution bathymetry [*Ladage et al.*, 2006] vividly illustrates impingement of elevated bathymetry associated with the fossil Wharton Ridge on the deformation front along the southern half of Nias, and it is likely that subduction of this elevated bathymetry has played an important role in long-term uplift of the island and perhaps even segmentation of megathrust ruptures along strike.

[10] Major intraplate faults that cut across and along the fore arc may have influenced the uplift history of Nias, but little is known about their recent rates of activity. The Mentawai fault, a major arc-parallel structure along the Mentawai islands south of Nias that may be primarily strike-slip [*Diament et al.*, 1992] or transpressive [*Sieh and Natawidjaja*, 2000] loses continuity at the latitude of Nias; a flexure along the east coast of the island may represent a strand of the Mentawai system that is primarily contractional at present (Figures 1 and 3) [*Karig et al.*, 1978; *Samuel and Harbury*, 1996; *Sieh and Natawidjaja*, 2000]. Long-term arc-parallel shortening may also be ac-

commodated by strike-slip faults that cross the fore arc, such as the Batee fault (Figure 1) [*Karig et al.*, 1978]. The Banyak islands north of Nias (Figure 1) are located in the middle of the fore-arc basin, and their presence reflects significant internal deformation of the fore arc along this stretch of the subduction zone.

[11] Despite the complex structural history of Nias, neotectonic surface deformation along active folds and faults is surprisingly subdued. Figure 3 summarizes the dominant active structures on Nias as interpreted from field observations and a digital elevation model derived from 30-m Shuttle Radar Topography Mission (SRTM) data [*Farr et al.*, 2007]. Limited resolution of the topographic data and thick tropical vegetation preclude rigorous analysis, but island topography is consistent with the dominance of low rate, and in many cases inactive, faults and folds. In general, emergent thrust faults and minor strike slip faults do not disrupt young surfaces or drainages, and folding appears to be the dominant deformational mechanism at work today over much of the island. The pattern of active faults and folds divides the island into two clear deformational domains. In the northwest, a series of closely spaced folds defined by recrystallized limestone surfaces plunges seaward. Holocene coral terraces and fluvial terraces along the flanks of these folds are not obviously warped or deformed, although the Holocene uplift and subsidence rates we obtain here (described below) are most easily explained by slow differential motion on these structures. In the southeast, a flexure that presumably overlies a steep west dipping thrust fault [*Moore and Karig*, 1980] along the east coast is the dominant recently active structure, although our observations suggest that significant deformation has now stepped onto thrust faults to the east that serve to lift the eastern coastal plain. Recent folding in the southeast is dominated by a doubly plunging antiform that defines the topographic spine of the island. Pronounced variations in surface geomorphology and coastal character accompany the northwest-to-southeast divide in active deformational styles of Nias. The northern half of Nias exhibits low mean elevations and subdued topography, in contrast to the rugged relief and 800+ m elevations in the south (Figure 3). Linear constructional coasts and offshore islands in the northwest give way to steep cliffs and scalloped coastal embayments in the southwest.

[12] The recent deformational history of Nias is preserved in the distribution and deformation of young coastal surfaces. Aside from active channels and floodplains, the youngest surfaces are fossil coral reefs and coastal chenier plains that are elevated relative to modern sea level (Figure 3). Our study focuses on prominent, uplifted Holocene fossil coral reefs that encircle much of the island. The reefs and associated recessional beach-sediment cover form surfaces that are typically flat, smooth, and continuous and are easily distinguished by their relative lack of dissection, their coastal position backing against a prominent erosional scarp, and their veneer of constructional beach berms and sparse in situ coral heads exposed at the surface.

3. The 2005 Coseismic Uplift Pattern

[13] The dominant feature of coseismic deformation in 2005 is a broad, simple antiform with a 2.5–2.9 m crest that parallels the island's northwest coast [*Briggs et al.*, 2006] (Figure 2). The trenchward decline in uplift indicates that significant coseismic slip did not reach the deformation front. Instead, significant afterslip appears to have occurred on the updip portion of the megathrust in the months after the 2005 rupture [*Hsu et al.*, 2006]. Toward the Sumatran mainland, coseismic uplift lessens nearly monotonically such that the line of zero uplift, or hinge line, nearly parallels the east coast. Uplift also decreases regularly along the southwest coast toward and around the southern end of the island. No compelling geologic or seismologic evidence for splay faulting was observed for the 2005 rupture and the uplift pattern is most simply explained by slip confined to the shallowly dipping (8°–12°) megathrust. The antiform and subsidence trough is consistent with predictions of elastic strain release due to slip on a buried low-angle thrust [*Savage*, 1983] and is similar to the pattern observed for other great megathrust ruptures [*Plafker*, 1965; *Plafker and Savage*, 1970]. At the outset of the present study, the observations that the welt of 2005 uplift is centered roughly on the island's west coast and that the hinge line runs roughly along the east coast led us to hypothesize that some increment of 2005 uplift might be retained as permanent deformation.

4. Determination of Uplift Rates

[14] Accurate measurements of tectonic deformation require that tectonic uplift is isolated from nontectonic contributions to vertical position. On Nias, we extract net tectonic uplift in the following manner:

$$\begin{aligned}[\text{Tectonic uplift}] = {} & [\text{Apparent uplift}] \\ & - [\text{2005 coseismic deformation}] \\ & - [\text{Holocene relative sea level variation}]\end{aligned}$$

In the simple equation above, "Tectonic uplift" represents the cumulative tectonic component of vertical deformation. The remaining terms of this equation, and the field and dating techniques we employ to convert elevation measurements at 22 sites to uplift rates, are described in detail below.

4.1. Apparent Uplift

[15] The height of corals and abandoned surfaces measured directly in the field incorporates all contributions to apparent vertical position (Figure 4). At most sites, we measure this apparent uplift by determining the elevation difference between modern low tide, as derived from a numerical tide model, and paleo–low tide as preserved by uplifted coral microatolls (Figure 4). This is a modification and extension of techniques previously applied to sea level studies [*Scoffin and Stoddart*, 1978; *Smithers and Woodroffe*, 2000], measurements of modern coseismic deformation [*Briggs et al.*, 2006; *Taylor et al.*, 1987, 1980] and reconstructions of paleoseismic uplifts [*Edwards et al.*, 1988].

[16] To establish a tide level datum on Nias, we use the numerical tide model NLOADF [*Agnew*, 1997] with appropriate regional constants [*Egbert and Erofeeva*, 2002] to generate tidal curves specific to each site. We define the lowest low tide (LLT) as the extreme lowest tide reached at

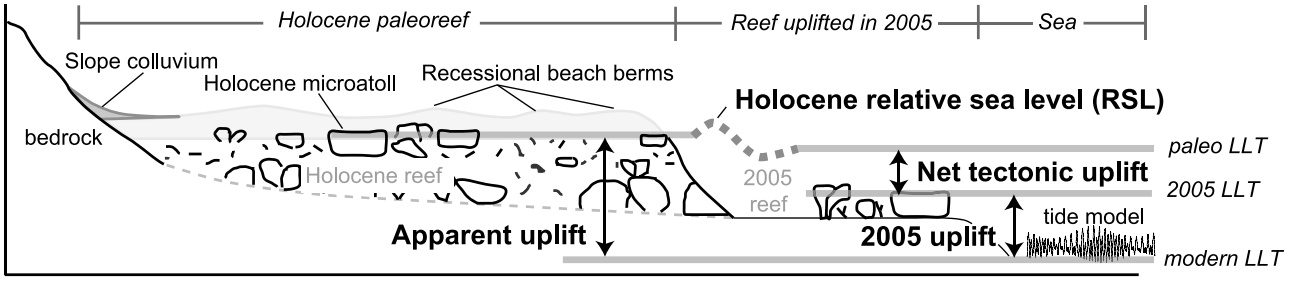

Figure 4. Schematic cross section through an uplifted Holocene reef illustrating major features and showing how net tectonic uplift is determined. See explanation in text.

each site during the 16 months prior to our visits. The modeled LLT value closely approximates the lowest spring tide observed on regional tide gauges [*Meltzner et al.*, 2006], which is the critical control on coral microatoll morphology [*Scoffin and Stoddart*, 1978; *Taylor et al.*, 1987; *Zachariasen et al.*, 1999]. Once established at a site, LLT provides a reliable and accurate datum from which we can reliably calculate the apparent heights of elevated features. A comparison of tide model predictions to tide gauge measurements in the 2004 Sumatran-Andaman M_w 9.2 rupture region found that they agreed to within ±0.1 m, which we adopt here as an estimate of modeled LLT error [*Meltzner et al.*, 2006].

[17] Several excellent proxies for paleo–low tide elevations are preserved on the uplifted paleoreefs of Nias. The best of these are the flat upper surfaces of *Porites* coral microatolls (Figure 5). Because their uppermost living tissues die with prolonged exposure to air and light, microatoll rim elevations reflect a systematic relationship to low tide levels to within a few centimeters [*Scoffin and Stoddart*, 1978; *Smithers and Woodroffe*, 2000; *Zachariasen et al.*, 1999]. Our previous studies have demonstrated that

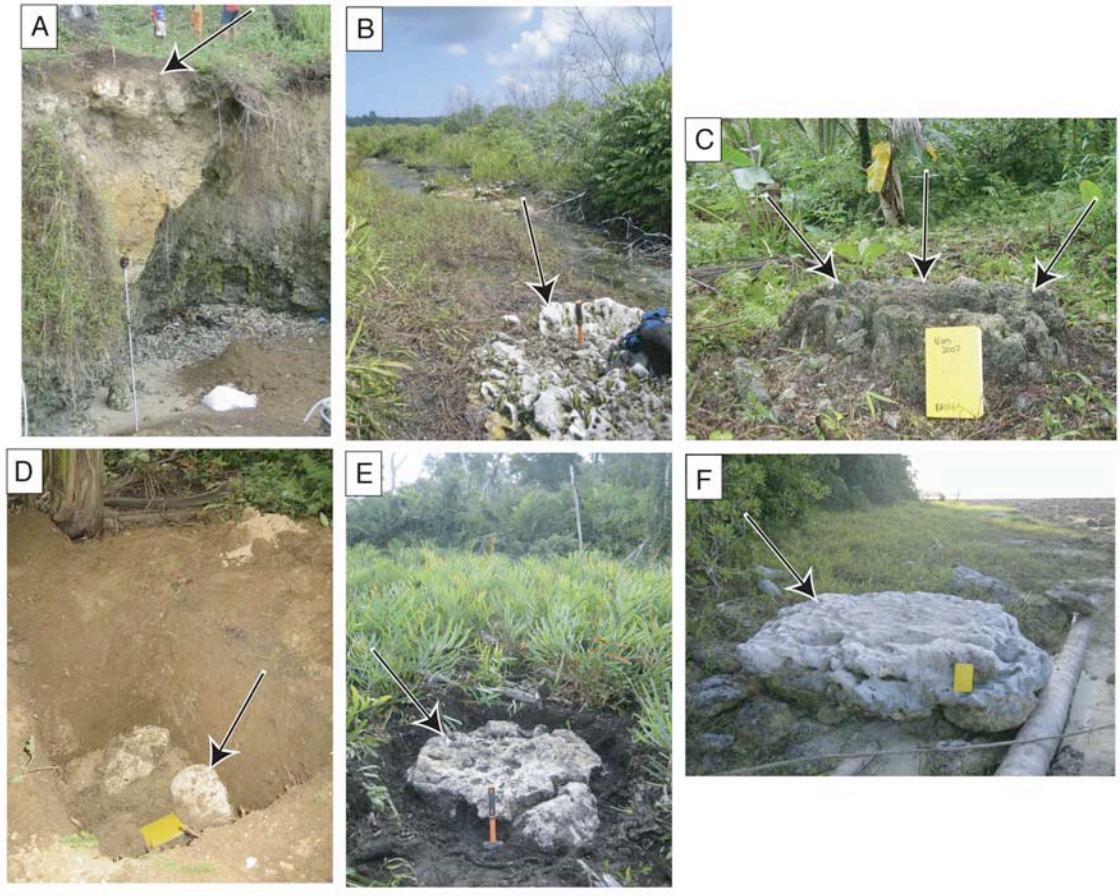

Figure 5. Photographs of typical Holocene microatolls (Figures 5a–5c, 5e, and 5f) and a nonmicroatoll (Figure 5d) defining the top of the Holocene reef flat. Arrows point to rims that record paleo–low tide or top of head. (a) Site GNGS (rod is 2.5 m). (b) Site LHWA (hammer is 40 cm). (c) Site HNKO (field book is 19 cm long). (d) Nonmicroatoll at site TDLU. (e) Site SIFI, head SIFI-B. (f) Site SIFI, head SIFI-C.

microatoll rim elevations are typically 4–5 cm higher than LLT elevations on Nias [*Briggs et al.*, 2006]. On uplifted paleoreefs, microatolls are frequently covered by recessional beach deposits or slope colluvium; thus wherever possible, we looked for *Porites* microatolls in cliffs and natural cut bank exposures. If not naturally exposed, we often uncovered them in shallow hand-dug pits.

[18] We use *Porites* microatolls as a proxy for paleo–low tide at eight sites. Because the uplift measurements are based on a comparison of present-day and paleo–low tide elevations, implicit in our approach is the reasonable assumption that the tidal range on Nias has remained similar (~0.7 m) throughout the Holocene. If the tidal range has been higher in amplitude in the past, then our uplift rates will be correspondingly lower because coral elevations are controlled by the elevation of low tide. The tops of the fossil microatolls we sampled were often slightly eroded, but we were unable to quantify the loss of material from these heads. Heads that we classify as microatolls retained significant original surface texture and exhibited the characteristic high width to height ratio of microatolls, and so we make the assumption that erosion of the heads we chose to sample is negligible. One exception is at site HLWA, where the *Porites* microatoll head was extremely eroded and may underestimate paleo–low tide by as much as 50 cm. Because we cannot quantify the erosion of the HLWA head, we consider the uplift rate a minimum there.

[19] In cases where fossil *Porites* microatolls were not available or not exposed, we turned to *Goniastrea* heads as paleo–low tide proxies. *Goniastrea* corals are useful because they yield reliable U-Th dates and are abundant on most raised Holocene reefs on Nias. We apply a small correction to account for the ability of *Goniastrea* microatolls to survive ~10 cm higher than *Porites* heads (Table 1 and Table S1 in the auxiliary material).[1] In cases where the microatoll morphology of the *Goniastrea* heads we sampled was ambiguous, we infer that these heads closely mark low-tide elevation based on their positions at the farthest landward portions of the paleoreef flat or on their occurrence in a field of similarly elevated heads defining the top of the reef flat. *Goniastrea* corals are the basis for uplift rates at six sites.

[20] We also utilized surface elevations of the Holocene terraces themselves to estimate uplift. We resort to this approach at seven sites where we are not able to obtain fossil coral heads, or where we could not confirm that fossil heads were in situ. This situation generally occurred where siliciclastic terrestrial sediment dominates the local depositional system, particularly on the southeast coast of Nias. Because constructional beach berms deposited during late Holocene regression can be several meters higher than the underlying reef flat on Nias, surface elevation measurements provide only a maximum bound on the uplift rate. A slight additional complication is the relief on the surface introduced by beach berms themselves, which can be as much as a meter at our sample sites. Despite these shortcomings, sites where we obtain simple surface elevations provide important qualitative observations that are useful for deducing the overall long-term uplift pattern on the island. Where possible, we demonstrate the Holocene age of the surface by dating organic material incorporated in associated deposits (Table S1). In most places the Holocene age of elevated berms is apparent from their continuity with adjacent uplifted reefs for which Holocene fossil coral ages have been obtained. To estimate uplift rates at these sites we assume an age of 6,500 ± 500 years for the landward edge of the elevated surface, consistent with the range of coral ages we obtain at similar positions at correlative sites along the Nias coast.

4.2. The 2005 Coseismic Deformation

[21] At each site we subtract from the uplift measurements coseismic vertical deformation that accompanied the 2005 megathrust rupture [*Briggs et al.*, 2006] (Figures 2 and 4). Because most sites are colocated with 2005 coseismic measurements, the application of this correction is straightforward. By removing this signal we restore microatolls and reef flats to the elevations they occupied while they formed in the years and decades prior to coseismic uplift in 2005. If the vertical deformation that occurred in 2005 is not accounted for, the long-term inelastic uplift pattern is contaminated, and apparently dominated, by the 2005 coseismic elastic signal. Inundation of cultural features on Nias in the decades prior to 2005, along with observations of pronounced interseismic subsidence along the Mentawai islands to the south prior to the 2007 ruptures there [*Sieh et al.*, 1999], suggests that most of the 2005 coseismic uplift along the Nias coast will be recovered before the next large megathrust event.

[22] Although removal of the 2005 uplift signal assumes that deformation in 2005 was purely elastic, it does not preclude the possibility that some fraction of uplift during previous megathrust ruptures was inelastic and permanent. Because the recurrence of 2005- and 1861-style ruptures appears to be frequent (nominally ~150 years) relative to the age of the uplifted surfaces (~2–7.3 ka), any inelastic component of previous megathrust slip has had many seismic cycles to accumulate.

4.3. Holocene Relative Sea Level Variation

[23] To determine net tectonic vertical deformation, we must also account for sea level variation during the Holocene. Nias is located in the far field [*Clark et al.*, 1978] of the major ice loads during the last glacial maximum and thus was subject to a mid-Holocene highstand of several meters or more. The highstand forms a common and clear feature of Indo-Pacific relative sea level (RSL) curves [*Dickinson*, 2001] and it is recorded by mid-Holocene emerged fossil coral reefs, elevated mangrove peats and muds, solution notches, and other mean sea level indicators along otherwise tectonically stable coasts. The far-field highstand is thought to have occurred when the global Holocene eustatic sea level rise slowed sufficiently so that solid earth processes, such as isostatic (ocean siphoning) and hydroisostatic (continental levering) processes, began to dominate the RSL record [*Mitrovica and Milne*, 2002].

[24] Geologic observations from the nearby relatively stable Malay-Thai peninsula provide clear evidence for a mid-Holocene RSL highstand in the region, but details of the timing and magnitude of the highstand, and how these vary spatially, are unclear. *Bird et al.* [2007] use mangrove

[1] Auxiliary materials are available in the HTML. doi:10.1029/2008JB005684.

Table 1. Holocene Uplift Rates

Site[a]	Sample[b]	Material[c]	Indicative Value[d]	Bound on Uplift Rate	Dating Method[e]	^{232}Th Age[f]	Apparent Uplift[g] (m)	2005 Coseismic Uplift[h] (m)	Raw Uplift Rate[i] (mm/a)	RSL Correction[j] (m)	Net Uplift[k] (m)	Net Uplift Rate[l] (mm/a)
BAWF	Holo surf	-	above LLT	max	inf	6500 ± 500	3.5 ± 0.5	−0.3 ± 0.3	0.58	1.88 ± 1	1.92	0.30 ± 0.21
BAWZ	Holo surf	-	above LLT	max	inf	6500 ± 500	10 ± 0.5	−0.25 ± 0.3	1.58	1.88 ± 1	8.37	1.29 ± 0.29
GLMB	Holo surf	-	above LLT	max	inf	6500 ± 500	11.5 ± 0.5	−0.3 ± 0.3	1.82	1.88 ± 1	9.92	1.53 ± 0.3
GNGS	GNGS-A	Porites micro	LLT	equal	U/Th	6390 ± 89	4.73 ± 0.1	0.24 ± 0.06	0.70	1.39 ± 1	3.1	0.49 ± 0.17
HGWL	Holo surf	-	above LLT	max	inf	6500 ± 500	4 ± 0.5	2.5 ± 0.06	0.23	1.62 ± 1	−0.12	−0.02 ± 0.22
HILN	HILN-A	Porites micro	LLT	equal	U/Th	5044 ± 101	3.36 ± 0.1	0.05 ± 0.06	0.66	1.6 ± 1	1.71	0.34 ± 0.21
HILD	HILD-A	Goni micro	above LLT	max	U/Th	6862 ± 46	3.68 ± 0.1	0.21 ± 0.06	0.51	1.35 ± 1	2.02	0.29 ± 0.15
HLWA	HLWA-E	Porites nonmicro	below LLT	min	U/Th	5523 ± 45	3.34 ± 0.1	−0.25 ± 0.16	0.65	1.02 ± 1	2.57	0.47 ± 0.17
HMAZ	Holo surf	-	above LLT	max	inf	6500 ± 500	4.75 ± 0.5	1.25 ± 0.16	0.54	1.88 ± 1	1.62	0.25 ± 0.23
HNKO	HNKO-A	Goni micro	above LLT	equal	U/Th	3804 ± 23	5.74 ± 0.1	1.75 ± 0.19	1.05	1.5 ± 1	2.39	0.63 ± 0.24
HUMN	HUMN-A	Porites micro	LLT	equal	U/Th	6529 ± 44	6.63 ± 0.1	0.24 ± 0.06	0.98	1.37 ± 1	5.02	0.77 ± 0.16
LAYA	LAYA-A	Goni nonmicro	below LLT	min	U/Th	3350 ± 22	1.64 ± 0.1	−0.1 ± 0.16	0.52	1.42 ± 1	0.32	0.10 ± 0.28
LGND	LGND-A	Porites micro	LLT	equal	U/Th	5982 ± 60	0.59 ± 0.1	0.78 ± 0.3	−0.03	0.93 ± 1	−1.12	−0.19 ± 0.13
LHWA	LHW-B	Porites micro	LLT	equal	U/Th	550 ± 63	1.36 ± 0.1	2.47 ± 0.3	−2.02	0.19 ± 1	−1.11	−2.02 ± 1.2
MBNA	Holo surf	-	above LLT	max	inf	6500 ± 500	7 ± 0.5	2.34 ± 0.16	0.72	1.62 ± 1	3.04	0.47 ± 0.24
MZL	MZL-2	Porites micro	LLT	equal	U/Th	1640 ± 30	3.17 ± 0.1	0.7 ± 0.23	1.51	0.67 ± 1	1.8	1.10 ± 0.55
SEN	SEN-2	Porites micro	LLT	equal	U/Th	4057 ± 255	2.59 ± 0.1	1.55 ± 0.16	0.26	1.62 ± 1	−0.58	−0.14 ± 0.22
SIFI	SIFI-C	Porites micro	LLT	equal	U/Th	2046 ± 27	1.45 ± 0.1	0.48 ± 0.06	0.47	0.84 ± 1	0.13	0.06 ± 0.51
SRMB	SRMB-A	Goni nonmicro	above LLT	max	U/Th	6764 ± 54	5.05 ± 0.1	2.56 ± 0.16	0.37	0.71 ± 1	1.78	0.26 ± 0.14
TDLU	TDLU-B	Goni nonmicro	below LLT	min	U/Th	6307 ± 45	4 ± 0.1	−0.25 ± 0.16	0.67	0.84 ± 1	3.41	0.54 ± 0.15
TETE	Holo surf	-	above LLT	max	inf	6500 ± 500	10.75 ± 0.5	−0.3 ± 0.3	1.70	1.88 ± 1	9.17	1.41 ± 0.29
WNGA	WNGA-2	Goni nonmicro	below LLT	min	U/Th	6270 ± 54	5.07 ± 0.1	1.81 ± 0.19	0.52	0.87 ± 1	2.39	0.38 ± 0.15

[a]See Figure 2 for site locations. Samples used to calculate uplift rates: see Table S1 in the auxiliary material for complete listing of dated material.
[b]Holo surf, age of Holocene surface assumed; other samples in Tables 2 and 3.
[c]Goni, Goniastrea; micro, microatoll.
[d]LLT, lowest low tide.
[e]U-Th dates reported in Table 2, ^{14}C dates reported in Table 3, and remaining are inferred (inf) maximum ages of Holocene surfaces.
[f]Age for all samples is reported here with respect to 2007.
[g]Noncorrected measurement of total apparent uplift.
[h]The 2005 coseismic uplift at site from *Briggs et al.* [2006].
[i]Uplift rate with only 2005 coseismic correction applied.
[j]Holocene RSL correction from *Peltier* [2004]; we apply an assumed uncertainty of ±1 m.
[k]Net uplift, apparent uplift minus 2005 coseismic uplift minus RSL correction.
[l]Net uplift rate, net uplift/^{232}T age. Uncertainties are estimated by including the full range of uncertainties for each value.

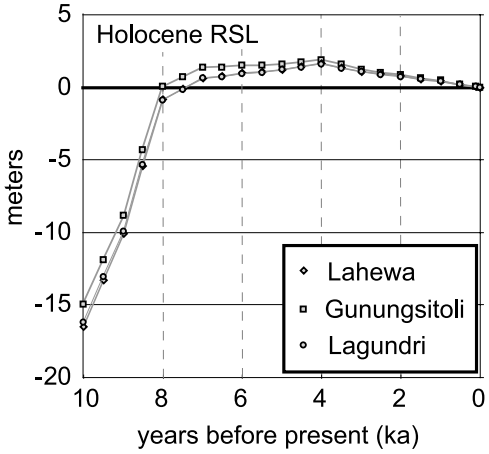

Figure 6. ICE-5G (VM2) predictions of the timing and magnitude of the Holocene relative sea level (RSL) on Nias [*Peltier*, 2004].

peats to demonstrate that sea level rose above modern average sea level at 7–7.5 ka in Singapore, and their data provide the most reliable limit available on the onset of the regional mid-Holocene highstand. The timing of the regional highstand peak is far less certain and is only loosely constrained to have occurred sometime between ~7–4 ka. Coral data from Phuket [*Scoffin and Le Tissier*, 1998] show a steady decline in RSL after ~6 ka. A more recent mid-Holocene RSL peak at 4850–4450 years B.P. has been interpreted from a carefully chosen set of Malay-Thai RSL data [*Horton et al.*, 2005], but unfortunately the data are sparse in the interval 4.5–6.5 ka, and the apparent peak is probably an artifact of combining observations from widely spaced shorelines subject to variable geophysical histories. Vita-Finzi and Situmorang [*Vita-Finzi*, 1995; *Vita-Finzi and Situmorang*, 1989] used a direct absorption technique for obtaining ^{14}C dates of shells collected from elevated surfaces on Nias and nearby Simeulue. The ages they obtained range from ~6.2–0 ka, suggesting that the highstand spans this time, although the lack of reliable paleosea level information and geological contexts for their samples does not allow for determination of the highstand peak timing and isolation of the tectonic contribution to apparent uplift.

[25] The magnitude of Holocene highstand peak varies regionally due to the spatially variable influences of hydro-isostasy [e.g., *Horton et al.*, 2005]. Because of this effect, observations from the stable Malay-Thai coast and the Malacca Straits that suggest mid-Holocene highstand peak elevations of ~5 m or more [*Geyh et al.*, 1979; *Tjia*, 1996] are not directly applicable to Nias. *Horton et al.* [2005] report a preliminary geophysical model that predicts 2–3 m of RSL change in the Holocene on Nias at about 6 ka, although they point out that an apparent mismatch between model results and the regional data they report may require future tuning of the model. In general, available geologic data point to a mid-Holocene highstand in the Nias region that begins at ~7 ka, reaches several meters, and extends well into the late Holocene.

[26] In the absence of independent geological data regarding the magnitude of the Holocene highstand on Nias, we turn to a global geophysical model of the predicted RSL curve to provide corrections to our uplift measurements. In particular, we use the predictions of the ICE-5G (VM2) model of global glacial isostatic adjustment [*Peltier*, 2004] as applied to Nias (R. Drummond and W.R. Peltier, personal communication, 2006). The curve for three representative sites on Nias is shown in Figure 6. The model predicts a rapid rise in RSL until ~7–8 ka, followed by a broad RSL highstand peaks of ~1.6–1.9 m at 4 ka before a steady drop in RSL to present-day sea level. This is roughly in accordance with regional geological observations and our own observations (detailed below and in the auxiliary material) which show that a highstand of several meters had begun by 7.3 ka and persisted until at least 2 ka. In the absence of observations free from tectonic influence, we take the ICE-5G (VM2) model to represent the best available constraint on Holocene RSL variation on Nias and we apply its predictions as corrections to each of our uplift sites (Tables 1 and S1). As GIA models evolve, we anticipate that their updated predictions can be applied as corrections to our uplift measurements.

4.4. Dating Methods

[27] We use the U-Th disequilibrium dating method to obtain ages from fossil coral heads [*Edwards et al.*, 1987; *Zachariasen et al.*, 1999]. The analyses were performed at the University of Minnesota and are shown in Table 1. This technique is particularly well suited for the analysis of coralline aragonite preserved in fossil corals [*Edwards et al.*, 2003]. We sampled portions of the fossil heads that retained pristine primary coralline structure and no visible evidence of recrystallization. A few samples contained elevated concentrations of initial ^{230}Th, which is reflected in the relatively higher uncertainty assigned to the sample ages (Table 1). The excess ^{230}Th in these heads may reflect contamination from detrital sources or unusual growth settings [*Zachariasen*, 1998] but the errors were not sufficient to require ischron corrections.

[28] We also obtained ^{14}C radiocarbon dates on in situ and reworked marine noncoralline carbonates and woody debris to constrain maximum surface ages and to provide control for stratigraphic sections (Table 2). To convert radiocarbon ages (B.P.) to calendar years (cal years B.P.), we used the reservoir ages and calibrations of *Fairbanks et al.* [2005] for marine samples and *Stuiver et al.* [1998] for terrestrial samples. To facilitate comparison of the 1950-based radiocarbon ages to the U-Th coral ages obtained in 2006–2007, we add 57 years to the calibrated radiocarbon ages and report them as "calendar ^{232}Th years B.P." (Table 3). Similarly, for coral samples dated with the U-Th method we also provide a column showing the correction of ^{232}Th ages calculated in 2006–2007 to years B.P., that is, with respect to 1950 (Table 2).

4.5. Strengths and Limitations of the Uplift Data

[29] Our uplift observations fall into three general types, and each type places slightly different bounds on uplift rates. The most robust measurements are from Holocene coral microatolls elevated with respect to a modern-tide-model-derived datum (10 sites; GNGS, HILD, HILN, HNKO, HUMN, LGND, LHWA, MZL, SEN, SIFI). A second class of uplift observations (5 sites; HLWA, LAYA,

Table 2. U-Th Analyses of Samples From Corals Used in This Study[a]

Sample	Chemistry Date A.D.	^{238}U (ppb)	^{232}Th (ppt)	$[^{230}Th/^{232}Th]$[b] (ppm)	$d^{234}U$ Measured[c]	$d^{234}U_{initial}$ Corrected[d]	$[^{230}Th/^{238}U]$ Activity[e]	^{232}Th Age Uncorrected	^{232}Th Age Corrected[f]	Age[g] (years B.P.)
BAWF-A	2007/07/28	2778 ± 4	13430 ± 37	156.8 ± 1.4	145.1 ± 2	146.8 ± 2.2	0.04589 ± 0.000401	4463 ± 41	4296 ± 172	4239 ± 172
GNGS-A	2006/08/20	4851 ± 10	10380 ± 25	508.0 ± 3.6	144.0 ± 3.3	146.7 ± 3.4	0.06583 ± 0.00046	6464 ± 50	6390 ± 89	6334 ± 89
GNGS-B	2006/11/20	2478 ± 3	273 ± 2	9469.5 ± 102.0	142.0 ± 1.8	144.5 ± 1.8	0.06319 ± 0.00038	6209 ± 39	6205 ± 40	6149 ± 40
GNGS-C	2006/08/20	2920 ± 5	1408 ± 5	2406.3 ± 16.3	143.3 ± 2.1	146.2 ± 2.2	0.07027 ± 0.00043	6917 ± 46	6901 ± 49	6845 ± 49
HILD-A	2006/11/20	2453 ± 3	297 ± 2	9506.1 ± 96.2	143.0 ± 1.9	145.8 ± 1.9	0.06974 ± 0.00044	6866 ± 46	6862 ± 46	6806 ± 46
HILD-B	2006/08/20	2513 ± 4	2401 ± 20	1236.7 ± 24.8	147.2 ± 2.2	150.2 ± 2.3	0.07156 ± 0.00131	7024 ± 133	6991 ± 137	6935 ± 137
HILN-A	2006/08/20	2603 ± 4	7162 ± 20	315.2 ± 2.1	141.4 ± 1.9	143.5 ± 1.9	0.05252 ± 0.00033	5139 ± 34	5044 ± 101	4988 ± 101
HILN-E	2006/11/20	2484 ± 3	267 ± 2	11409.7 ± 96.1	142.4 ± 1.8	145.4 ± 1.8	0.07420 ± 0.00043	7324 ± 46	7320 ± 46	7264 ± 46
HILN-F	2006/08/20	2356 ± 4	997 ± 4	2425.5 ± 13.8	145.6 ± 2.1	148.1 ± 2.2	0.06217 ± 0.00030	6086 ± 32	6071 ± 35	6015 ± 35
HLWA-D	2006/11/20	2384 ± 3	105 ± 2	21148.7 ± 443.3	143.5 ± 1.6	145.7 ± 1.7	0.05644 ± 0.00029	5522 ± 30	5520 ± 30	5464 ± 30
HLWA-E	2006/08/20	2196 ± 3	236 ± 3	8699.7 ± 121.3	145.1 ± 2.1	147.4 ± 2.2	0.05657 ± 0.00044	5527 ± 45	5523 ± 45	5467 ± 45
HMAZ-A	2007/07/16	2655 ± 4	3794 ± 12	35.5 ± 0.9	148.2 ± 2	148.3 ± 2.1	0.00308 ± 0.000074	293 ± 7	243 ± 50	186 ± 50
HNKO-A	2007/07/16	2419 ± 4	82 ± 4	19183.9 ± 984.6	145.4 ± 2	147.0 ± 2.1	0.03925 ± 0.000226	3805 ± 23	3804 ± 23	3747 ± 23
HNKO-B	2007/07/16	2580 ± 4	10643 ± 33	242.8 ± 2.3	148.2 ± 2	150.7 ± 2.3	0.06064 ± 0.000545	5918 ± 56	5776 ± 153	5719 ± 153
HUMN-A	2007/07/16	2864 ± 5	2328 ± 7	1356.3 ± 7.2	144.6 ± 2	147.2 ± 2.2	0.06679 ± 0.000315	6557 ± 34	6529 ± 44	6472 ± 44
LAYA-A	2006/11/20	2387 ± 3	53 ± 2	25515.4 ± 952.8	142.0 ± 2.0	143.4 ± 2.0	0.03453 ± 0.00021	3351 ± 22	3350 ± 22	3294 ± 22
LAYA-D	2006/08/20	2999 ± 4	41861 ± 278	82.5 ± 1.6	145.9 ± 1.9	148.5 ± 2.0	0.06977 ± 0.00124	6851 ± 126	6368 ± 500	6312 ± 500
LGND-A	2007/07/28	2870 ± 5	4099 ± 9	712.2 ± 3.9	145.1 ± 2	147.6 ± 2.2	0.06160 ± 0.000321	6031 ± 34	5982 ± 60	5925 ± 60
LHWA-A	2007/07/16	2549 ± 4	3142 ± 9	259.2 ± 2.5	147.2 ± 2	147.9 ± 2.2	0.01935 ± 0.000180	1857 ± 18	1815 ± 46	1758 ± 46
LHWA-B	2006/09/24	2717 ± 4	4689 ± 15	61.0 ± 1.8	144.7 ± 2.0	145.0 ± 2.0	0.00637 ± 0.00019	610 ± 18	550 ± 63	494 ± 63
MBNA-A	2006/11/20	2311 ± 3	196 ± 2	1642.4 ± 25.8	147.9 ± 1.8	148.2 ± 1.8	0.00842 ± 0.00010	804 ± 10	801 ± 10	745 ± 10
MBNA-B	2006/11/20	3373 ± 4	264 ± 2	1789.6 ± 29.4	146.7 ± 1.5	147.0 ± 1.5	0.00847 ± 0.00012	809 ± 12	807 ± 12	751 ± 12
MZL-2	2006/08/20	2300 ± 3	1813 ± 3	364.0 ± 2.6	147.0 ± 1.9	147.7 ± 1.9	0.01738 ± 0.00012	1667 ± 12	1640 ± 30	1584 ± 30
MZL-6	2006/09/24	2174 ± 3	2521 ± 8	356.0 ± 4.8	147.0 ± 2.3	148.0 ± 2.3	0.02500 ± 0.00033	2406 ± 32.0	2366 ± 51	2310 ± 51
MZL-7	2006/09/24	2692 ± 3	1615 ± 5	1187.7 ± 21.0	144.7 ± 1.8	146.4 ± 1.8	0.04461 ± 0.00040	4337 ± 39.8	4316 ± 45	4260 ± 45
SEN-2	2006/09/24	2710 ± 3	19461 ± 64	101.7 ± 1.3	143.5 ± 1.8	145.1 ± 1.8	0.04424 ± 0.00054	4306 ± 54	4057 ± 255	4001 ± 255
SIFI-A	2006/08/20	2853 ± 4	27550 ± 128	114.0 ± 1.5	145.3 ± 2.0	147.8 ± 2.0	0.06668 ± 0.00081	6543 ± 82	6208 ± 345	6152 ± 345
SIFI-B	2006/11/20	2744 ± 3	2267 ± 5	1141.5 ± 6.7	143.6 ± 1.7	145.8 ± 1.7	0.05712 ± 0.00032	5590 ± 33	5561 ± 44	5505 ± 44
SIFI-C	2006/08/20	2451 ± 3	1736 ± 4	502.9 ± 2.9	147.8 ± 1.9	148.6 ± 1.9	0.02157 ± 0.00012	2071 ± 12	2046 ± 27	1990 ± 27
SRMB-A	2006/11/20	1806 ± 2	1517 ± 4	1357.7 ± 9.1	144.2 ± 1.7	147.0 ± 1.7	0.06909 ± 0.00043	6793 ± 45	6764 ± 54	6708 ± 54
TDLU-B	2006/11/20	2462 ± 3	485 ± 2	5395.1 ± 41.8	144.5 ± 1.9	147.1 ± 1.9	0.06437 ± 0.00042	6314 ± 44	6307 ± 45	6251 ± 45
WNG-1	2006/08/20	2207 ± 3	487 ± 3	564.6 ± 7.4	143.3 ± 1.8	143.6 ± 1.8	0.00754 ± 0.00009	722 ± 9	715 ± 12	659 ± 12
WNG-2	2006/09/24	2671 ± 3	263 ± 2	10723.3 ± 128.4	142.6 ± 1.8	145.1 ± 1.8	0.06386 ± 0.00052	6273 ± 53	6270 ± 54	6214 ± 54

[a] Analytical errors are 2σ of the mean.

[b] The degree of detrital ^{230}Th contamination is indicated by the $[^{230}Th/^{232}Th]$ atomic ratio instead of the activity ratio.

[c] The $\delta^{234}U = ([^{234}U/^{238}U]_{activity} - 1) \times 1000$.

[d] The $\delta^{234}U_{initial}$ corrected was calculated based on ^{230}Th age (T), i.e., $\delta^{234}U_{initial} = \delta^{234}U_{measured} X e^{\lambda 234 * T}$, and T is corrected age.

[e] $[^{230}Th/^{238}U]_{activity} = 1 - e^{-\lambda 230 T} + (\delta^{234}U_{measured}/1000)\,[\lambda_{230}/(\lambda_{230} - \lambda_{234})](1 - e^{-(\lambda 230 - \lambda 234)T})$, where T is the age. Decay constants are 9.1577×10^{-6} a^{-1} for ^{230}Th, 2.8263×10^{-6} a^{-1} for ^{234}U, and 1.55125×10^{-10} a^{-1} for ^{238}U [*Cheng et al.*, 2000].

[f] Age corrections were calculated using an estimated $^{230}Th/^{232}Th$ atomic ratio of 6 ± 6 ppm.

[g] Age in years B.P. with respect to 1950.

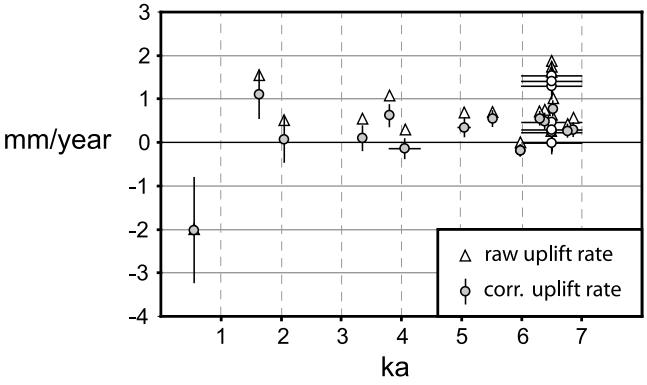

Figure 7. Plot showing the effect of applying model RSL corrections to uplift rates. Triangles represent uncorrected rates, and circles represent corrected rates and uncertainties. Open circles are uplift sites with assumed ages.

SRMB, TDLU, WNGA) relies on elevated nonmicroatoll corals that closely approximate (to within tens of centimeters) the elevation of paleo–low tide, and these measurements place close minimum constraints on uplift rates. A third type of observation is obtained along the southeast and southwest coasts where modern and paleoreefs are rare (7 sites; BAWF, BAWZ, GLMB, HGWL, HMAZ, MBNA, TETE); these measurements rely on the elevation of sandy berm complexes and assumed mid-Holocene ages for the surfaces, and are likely to slightly overestimate Holocene uplift rates. Finally, at three sites (DHNA, FOFO, and ONLB) we obtained only qualitative estimates of uplift.

[30] The primary source of uncertainty in our uplift rate calculations stems from the model correction that must be applied for Holocene RSL variation. The ICE-5G (VM2) model Holocene RSL curve predicts a maximum sea level of 1.9 m at 4 ka, to which we assign a ±1 m uncertainty on the basis of the prediction of ~1 m of variation between adjacent sites on Nias at 7 ka (Figure 6). Application of this model to our uplift observations reduces uplift rates (Figure 7). Also, application of the model sea level curve correction results in apparent slow subsidence at sites that otherwise would appear to be stable or uplifting very slowly. On the basis of coastal geomorphology, it appears that most of these sites are indeed stable or slowly subsiding, but confirmation of this awaits a consensus Holocene RSL curve for Nias.

5. Study Sites

[31] Elevated Holocene surfaces along the Nias coast are readily identified on the basis of their coastal position, their relative lack of dissection, and their level and often continuous surfaces. Holocene terraces range from tens of meters to several kilometers in width, and because they adjoin the sea, they are often substantially modified by human activity. Pristine surfaces are usually composed of well-preserved beach berms, back-berm depressions with locally derived basin fill, and in situ fossil coral heads or reworked coral heads and clasts. The Holocene surfaces we describe here are set into paleosea cliffs and steep slopes formed in older, higher material that we describe broadly as "bedrock." In some cases, the landward material is recrystallized reef limestones, but often it is siltstone or sandstone. In all cases the contact between the inset fringing Holocene reef and the older material along a paleosea cliff or slope is clear. Our technique does not rely on identification and correlation of shoreline angles, but we extended our surveys to the landward edge of the terraces wherever possible, that is, to the shoreline angle position, to fully characterize the age and extent of the Holocene surface.

[32] At each site, we surveyed the elevation of coastal features using an electronic total station surveying instrument, usually along transects cut by machete through forests or plantations. We mapped relevant surfaces and surficial features using the total station, handheld GPS, and occasionally pace-and-compass techniques, augmented by high-resolution satellite imagery where available. We took advantage of natural coral exposures in sea cliffs or stream cuts, and usually supplemented these with hand-dug excavations.

[33] In this section, we illustrate the techniques we used to determine net Holocene tectonic uplift rates at 22 sites along the Nias coast. In the main body of the paper, we focus on ten sites that convey the range of features we encountered and the measurement and dating methods we used. To keep detail at a minimum here, we present the results from 12 additional uplift rate sites in the auxiliary material, where we also include an additional three sites (ONLM, DHNA, and FOFO) that provide qualitative evidence of uplift.

5.1. SRMB (Sirombu)

[34] Site SRMB sits on the western edge of the low headland that controls the prominent tombolo at Sirombu (Figures 2 and 8). A well-preserved Holocene surface composed of sandy beach berms and sparse in situ coral heads laps onto a low (~15 m) siltstone ridge that forms the core of the headland. Coseismic uplift of 2.56 m here in 2005 exposed an abrasion platform up to 250 m wide, covered with rare coral heads and microatolls. The relative lack of massive corals here, both modern and fossil, probably reflects the high-energy surf conditions at the site.

[35] We excavated a pit to the underlying bedrock abrasion platform that exposed beach sands atop cemented coral rubble and small (~0.3 m), apparently in situ *Goniastrea* coral heads. We assume the heads were in situ because they were in growth position and rooted in cemented reef-rock substrate; however, it is also possible that these heads were reworked and only apparently in original position. The age of sample SRMB-A, 6764 ± 54 years, is consistent with dated in situ coral heads in similar positions near the shoreline angle at several other sites.

[36] Because sample SRMB-A is not a microatoll, it places a minimum constraint on total apparent uplift of 5.05 m. But because the head is located nearly at the shoreline angle we are confident that it marks paleo–low tide elevation to within tens of centimeters. Subtraction of 2005 coseismic uplift (2.56 m) and the correction for mid-Holocene sea level (0.71 m) results in a net uplift value of 1.78 m, corresponding to a net uplift rate of 0.26 ± 0.14 mm/a.

5.2. WNGA (Pulau Wunga)

[37] Wunga is a small island 13.5 km off the northwest coast of Nias (Figures 2 and 9). During the long period of

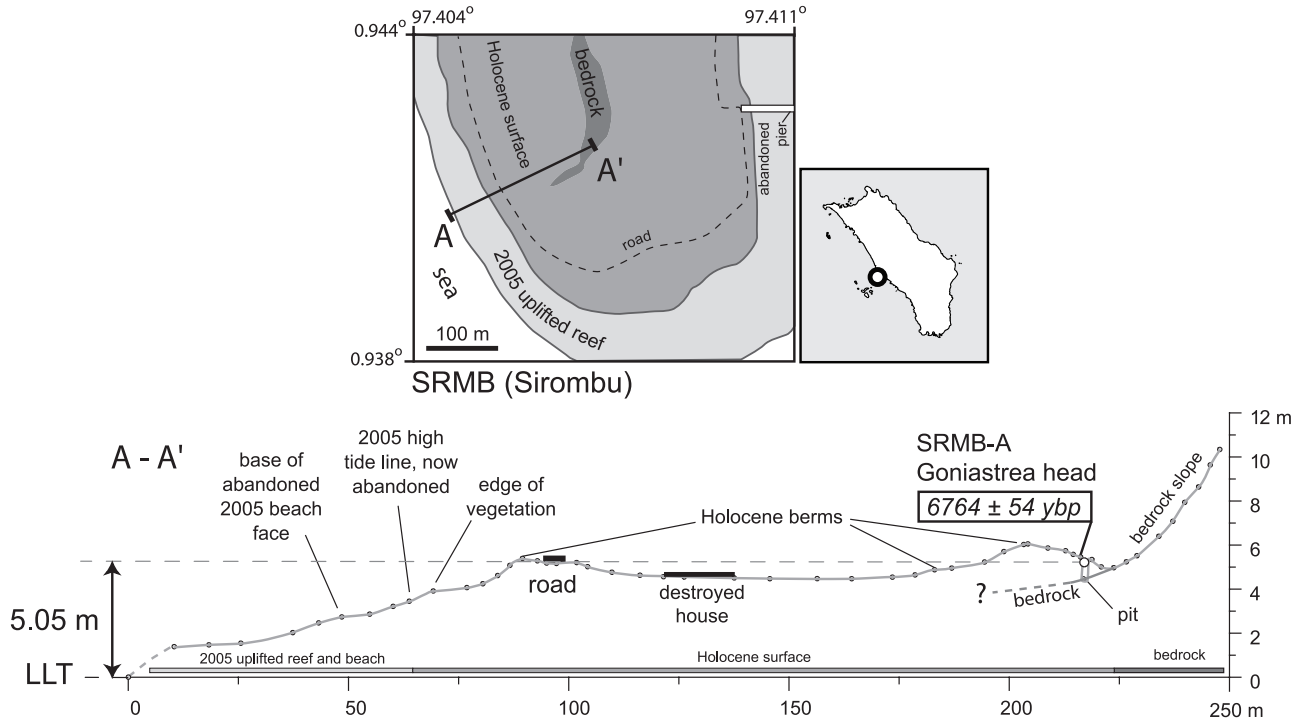

Figure 8. Surficial geologic map and topographic profile at site SRMB. Site locations for Figures 8–17 are indicated in Figure 2 and in accompanying insets.

subsidence prior to 2005, the island was divided in two by the slowly rising waters of a central lagoon. Sudden uplift of ~1.8 m in 2005 reunited the western half of Wunga and nearly closed off the eastern lagoon entrance.

[38] We surveyed surficial features near the southeastern tip of the pre-2005 entrance to the central lagoon. A low, sandy Holocene surface with well-preserved berms forms most of the island, with the exception of a few isolated older limestone knobs ~12–15 m high that are composed of entirely recrystallized coralline limestone of unknown age.

[39] We measured three topographic profiles at the site. Profile A-A′ extends onto an elevated surface with many in situ *Goniastrea* heads. A nonmicroatoll *Goniastrea* head (WNGA-2) along transect A-A′ yields an age of 6270 ± 54 years. When corrected for 2005 coseismic uplift and Holocene RSL variation, this head yields an uplift rate of 0.38 ± 0.15 mm/a. The sampled head is not a microatoll, but it marks the top of an extensive paleoreef flat and thus represents a minimum uplift rate that closely approximates the actual rate.

[40] Profiles B-B' and C-C' cross lower, younger Holocene berms. Excavation into a back-berm swale exposed an apparently in situ *Goniastrea* microatoll (sample WNGA-1) rooted in cemented coral rubble. The age we obtained from this head, 715 ± 12 years, was unexpectedly young and it raises the possibility that this head may have been a tsunami block that was only apparently in situ. The similarity in age and back-berm swale position of sample WNGA-1 to heads at site MBNA (see the auxiliary material) strengthens this possibility, although confirmation awaits more detailed paleoseismic work in the region. If the head was indeed in situ, it corresponds to an uplift rate of 0.28 ± 1.28 mm/a. The large uncertainty is due to the large error that we assign to the Holocene RSL estimate (0.27 ± 1 m).

[41] It is possible that the low knobs (~15 m or lower) of recrystallized coralline limestone on Wunga were deposited during the stage 5e interglacial period (~120–130 ka). Assuming the coral formed at sea level at the time, sustained uplift of 0.38 mm/a would raise the paleoreefs to ~50–55 m. This is not observed, and thus the current uplift rate of 0.38 mm/a began sometime after ~125 ka, suggesting that Wunga island is young.

5.3. GLMB (Golumbanua)

[42] Site GLMB (Figure 2) is representative of several sites on the southeast coast of Nias that show clear evidence for Holocene uplift, but for which we are unfortunately unable to obtain uplift rates based on elevated paleoreefs. The transect at Golumbanua (Figure 10) extends across a broad, elevated platform that is continuous with the extensive coastal plain to the north and an elevated Holocene terrace to the south. The Golumbanua surface rises gently and consistently from sea level to ~11.5 m where it abuts a bedrock slope. The surface is composed of clearly defined sets of beach berms (designated as Holocene surfaces 1–3 on Figure 10) that give way to more muted topography not readily differentiated into discrete berm sets (Holocene surface 4). A wedge of clay-rich slope colluvium mantles the landward edge of the elevated surface.

[43] Like several other sites on the southeastern coast of Nias, site GLMB lacks modern coral due to a modern depositional system that is dominated by abundant sediment input from the Nias highlands and suspended sediment from the shallow strait. To place a maximum constraint on the age of the uplifted surface, we obtained a single radiocarbon

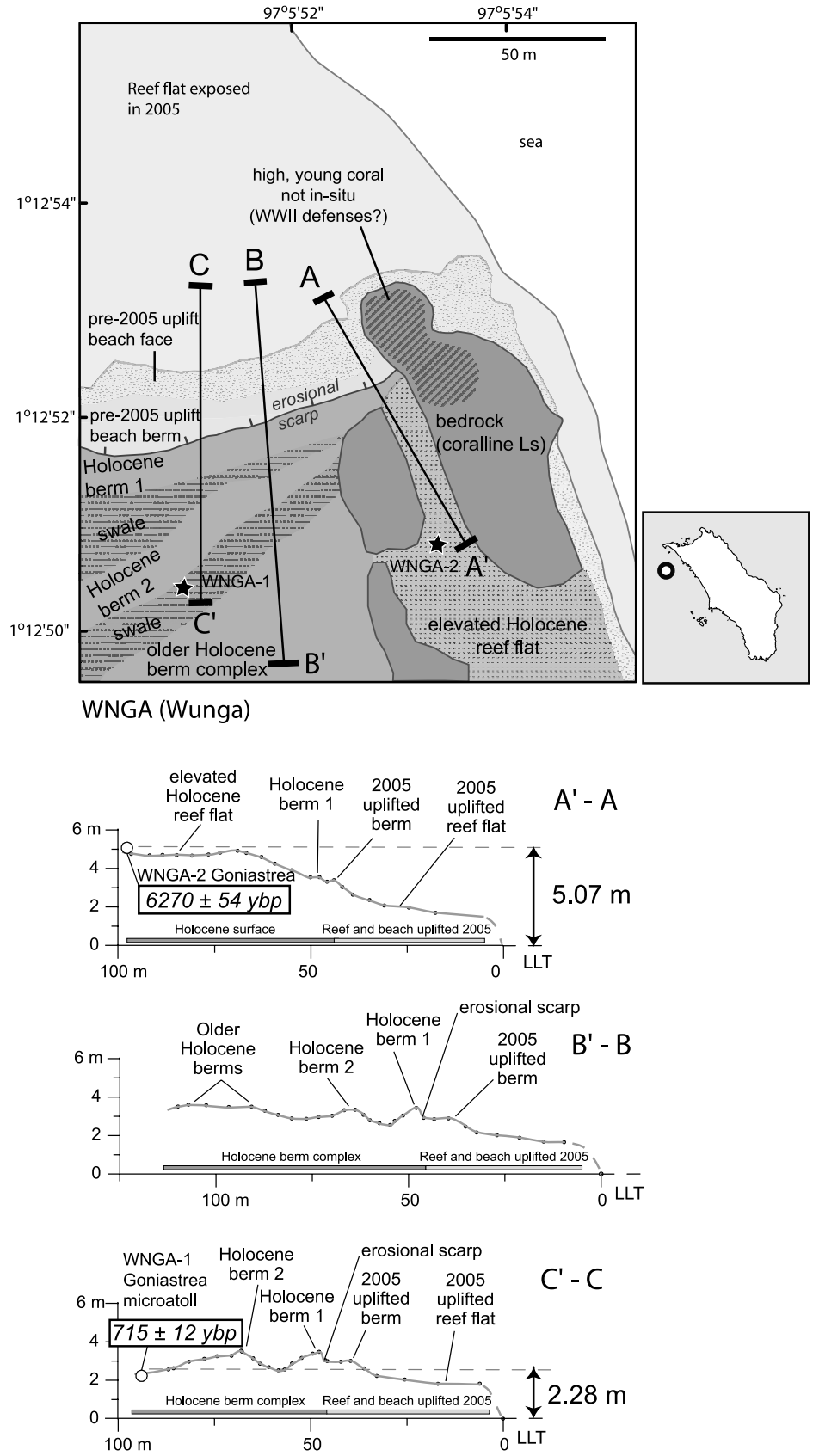

Figure 9. Surficial geologic map and topographic profiles at site WNGA.

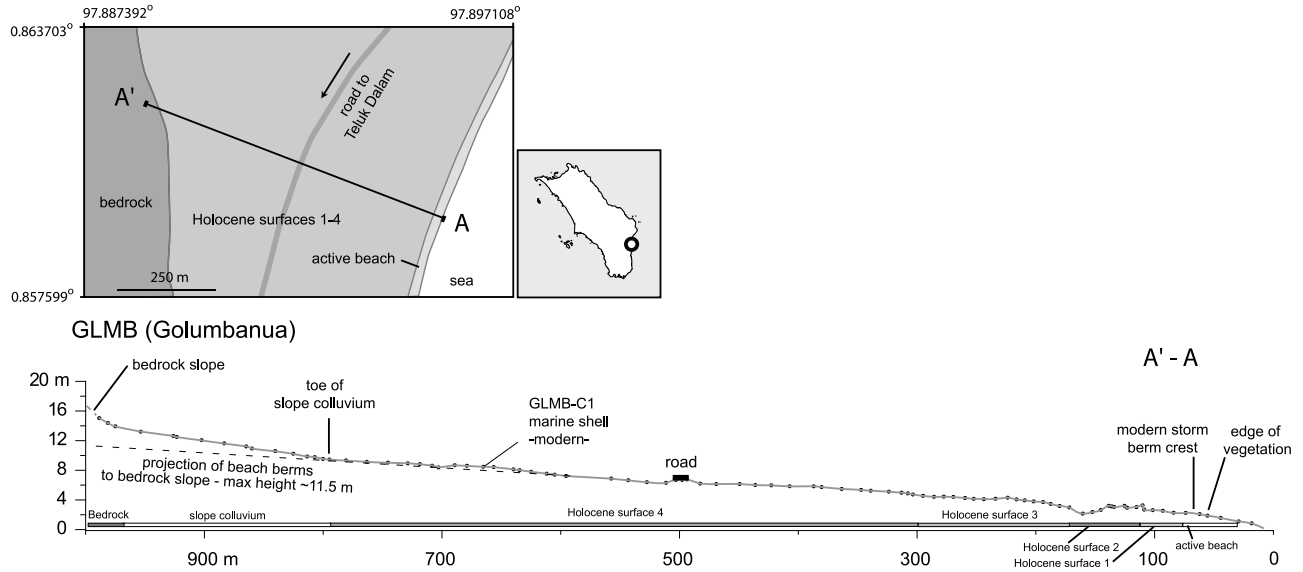

Figure 10. Surficial geologic map and topographic profile at site GLMB.

date from a gastropod recovered from a pit excavated near the landward edge of the transect. Unfortunately, the sample yielded a modern age, and thus must reflect young material reworked deep into the beach sands that compose the deposit. In this case, and at sites with similar characteristics (e.g., TETE; see the auxiliary material), we infer a maximum age for the surface of 6500 ± 500 years. This inference is supported by a clear correlation between the GLMB surface and dated Holocene surfaces to the south, and the age range of the highest, oldest coral heads we encountered throughout the island. The GLMB surface reaches to ~11.5 m elevation above LLT when projected beneath slope colluvium at the rear of the transect, and so we obtain a maximum uplift rate estimate of 1.53 ± 0.3 mm/a here.

[44] The gentle, continuous seaward slope of the surface and the lack of clear sequentially uplifted and abandoned surfaces suggests that uplift has been slow and steady, rather than infrequent and episodic during the Holocene. Similar sloped surfaces extending along the east coast from site HILN to site BAWZ (Figure 2) reflect a zone of the highest Holocene uplift rates on Nias. The gentle seaward slope of the surfaces along this zone is in sharp contrast to sites on the northern coast, where the upraised Holocene fringing reefs are generally broad and level.

5.4. LHWA (Lahewa)

[45] Site LHWA (Figure 2) is a striking example of locations that experienced substantial uplift in 2005 but have been subject to net subsidence in the longer term. The site is located on a small peninsula on the east side of Lahewa harbor in northwest Nias. The peninsula was covered by a dense mangrove forest that flooded at high tide prior to 2005 (Figure 11). Coseismic uplift in 2005 killed the mangrove forest and caused the peninsula to nearly double in size. Uplift of 2.47 m in 2005 exposed mangrove peats, muds, and massive corals and microatolls on an extensive coral abrasion surface.

[46] We obtained a U-Th date of 550 ± 63 years on a 1.5 m diameter *Porites* microatoll exposed in a small tidal channel and sitting directly on the abrasion surface (Figure 5b). This head is especially interesting because it records a paleo–low tide level that is more than 1.1 m lower than low tide levels immediately before uplift in 2005. The relationship between pre-2005 LLT and paleo-LLT obtained from the sampled microatoll requires ~1.1 m of subsidence at the site since ~550 years ago (Figure 11). Because the head is firmly attached to a carbonate strath surface it is unlikely that the subsidence is due to sediment compaction. The overall stratigraphy of the site also reflects recent subsidence: The coral abrasion platform is covered by large coral heads, which in turn are overlain by mangrove peats. We bracketed the timing of abrasion platform burial by obtaining AMS ^{14}C dates from a mollusc shell embedded in the strath surface, and also from the base of the overlaying peats. These samples bracket the burial of the abrasion surface and dated microatoll to 300–350 years ago, consistent with recent rapid subsidence of the site.

[47] Net Holocene subsidence at site LHWA is consistent with the geomorphic character of the NW corner of Nias and the structural position of Lahewa harbor in the trough of a small syncline (Figure 3). Elevated Holocene terraces are absent near Lahewa, and the scalloped coastline hosts mangrove forests that abut bedrock slopes of completely recrystallized limestone. The elevated limestone indicates that emergence was dominant at LHWA prior to recent net subsidence.

5.5. SIFI (Sifahandro)

[48] Site SIFI is on the western edge of Teluk Siabang (Siabang Bay), approximately 3 km east of the nearby village of Sifahandro. The site is on a level, platform of over 1 km in width (Figure 12).

[49] We obtained the ages and precise elevations of two microatolls near the coast. The two heads are similar in elevation but return substantially different ages. Sample SIFI-C (2046 ± 47 years) is from a *Porites* microatoll that was in the intertidal zone prior to 0.48 m of uplift here in 2005 (Figure 5f). Sample SIFI-B (5561 ± 44 years) is from a

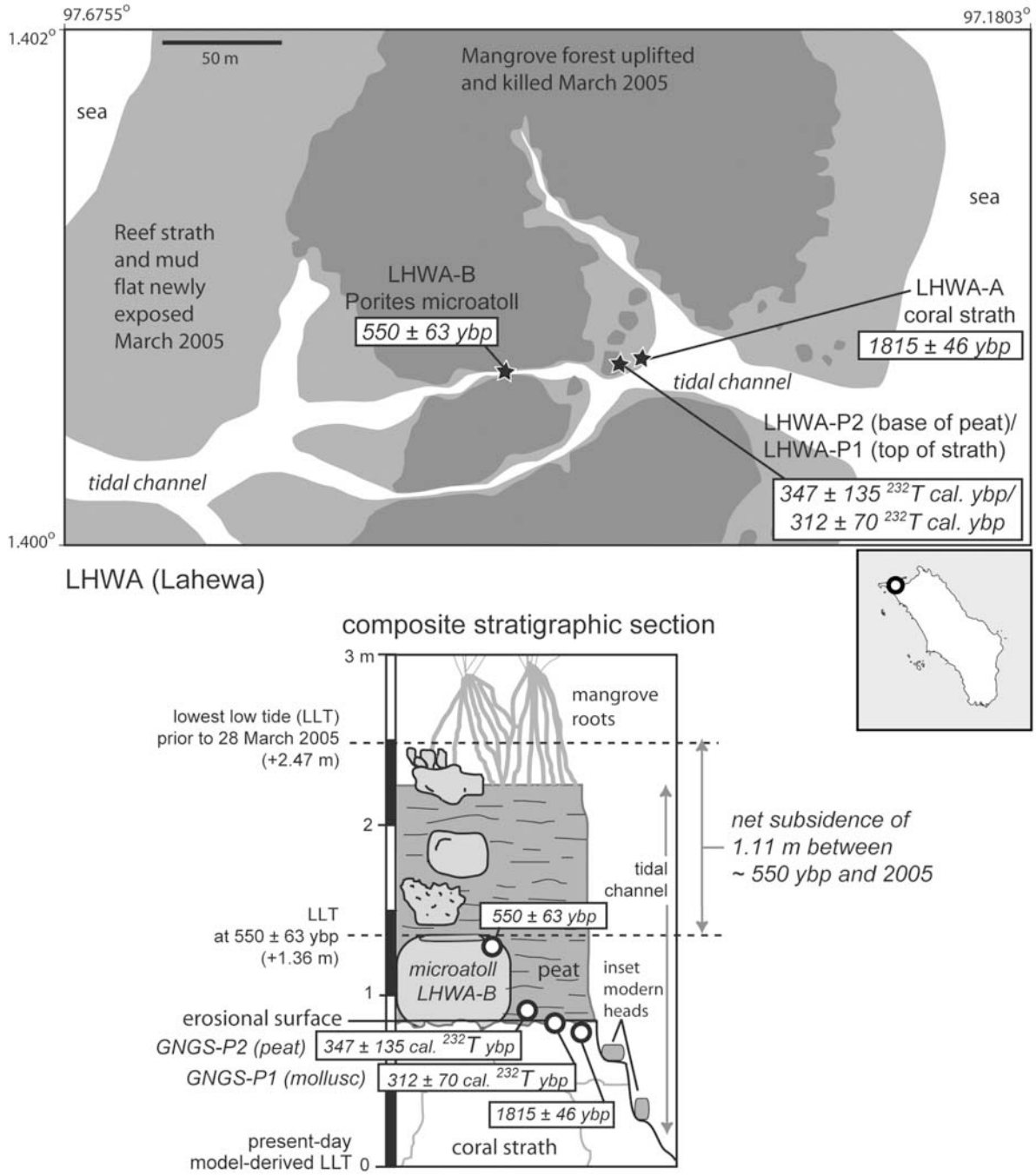

Figure 11. Surficial geologic map and composite stratigraphic section at site LHWA.

microatoll we exposed in a pit ~100 inland from the 2005 coastline (Figure 5e).

[50] We also obtained a date and elevation estimate from the farthest inland undisturbed head that we could find. Coral is exposed intermittently along the terrace surface between the coast and a point nearly 1 km inland, where we sampled this in situ nonmicroatoll *Porites* head (SIFI-A). Its age, 6208 ± 345 years, is similar to the ages of the farthest inland heads at most of our other sites. Although we could not obtain precise elevation control on this head, an altimeter transect showed no elevation change between samples SIFI-A and SIFI-B and so we assume they are the same elevation within error of the altimeter (±2 m).

[51] The similarity in elevations for these three heads and their wide range of ages suggests that the elevated paleoreef here records a long period of relative sea level stability, from at least ~6200 (the age of the oldest, most landward head) to ~2000 years ago. When corrections for 2005 coseismic uplift and Holocene RSL are applied, we obtain an uplift rate of 0.06 ± 0.51 mm/a. This rate is close to zero and, when coupled with the geomorphology of the reef, it suggests that the entire terrace surface records only minimal tectonic uplift. Instead, the dominant signal recorded by the

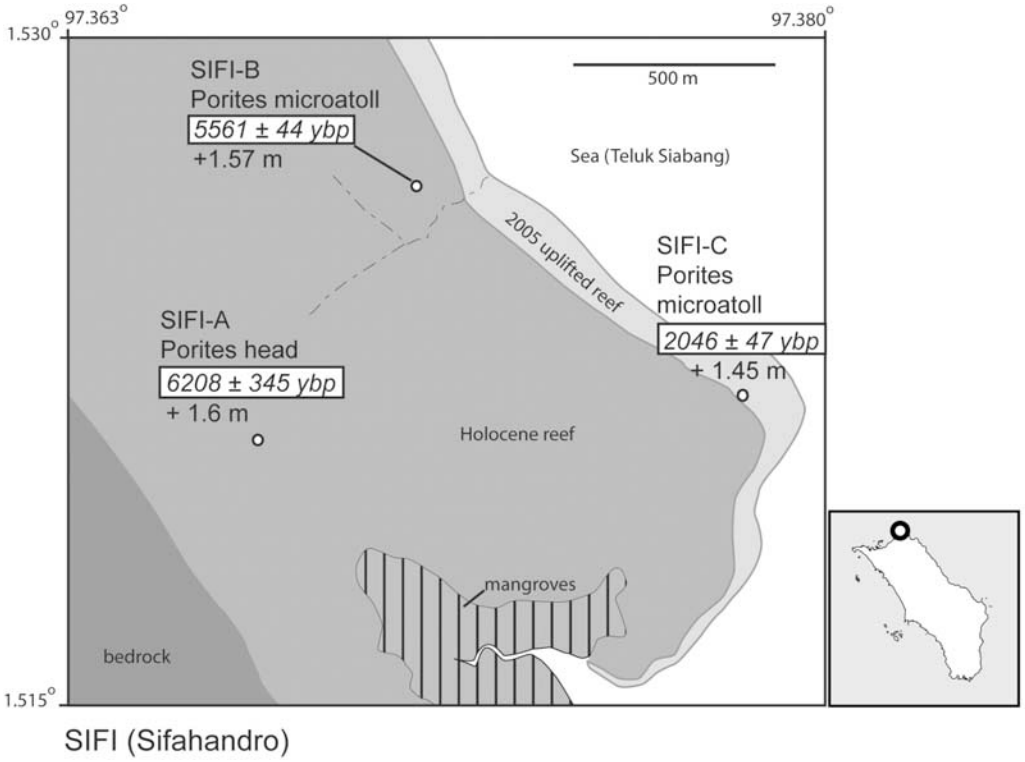

Figure 12. Surficial geologic map at site SIFI.

surface is abandonment after a broad, low-amplitude mid-Holocene RSL highstand.

5.6. HILD (Hiliduruwa)

[52] Site HILD is near the northern tip of Nias north of Hiliduruwa village on an extensive ~ 0.4 km wide reef platform (Figures 2 and 13). Conspicuous and abundant in situ coral heads and microatolls sit on the platform. A few low beach berms overlie the corals, presumably reflecting regression from the reef-forming highstand or perhaps progradation of the shoreline during a sustained mid-Holocene highstand. In addition to the in situ heads, numerous large coral heads appear to have been deposited as erratics on the surface and these may represent tsunami blocks.

[53] We obtained U-Th dates on two of the highest, most landward in situ coral heads. Sample HILD-A (6862 ± 47 years) is a 0.75 m wide *Goniastrea* microatoll, and HILD-B (6991 ± 137 years) is a nonmicroatoll *Porites*

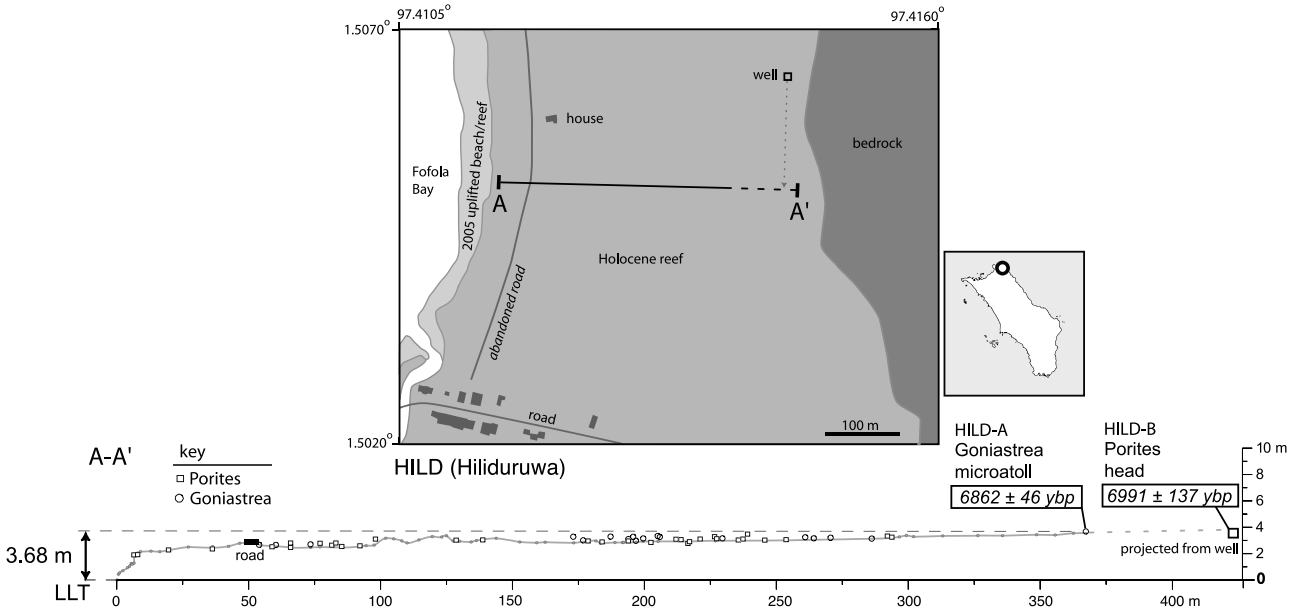

Figure 13. Surficial geologic map and topographic profile at site HILD.

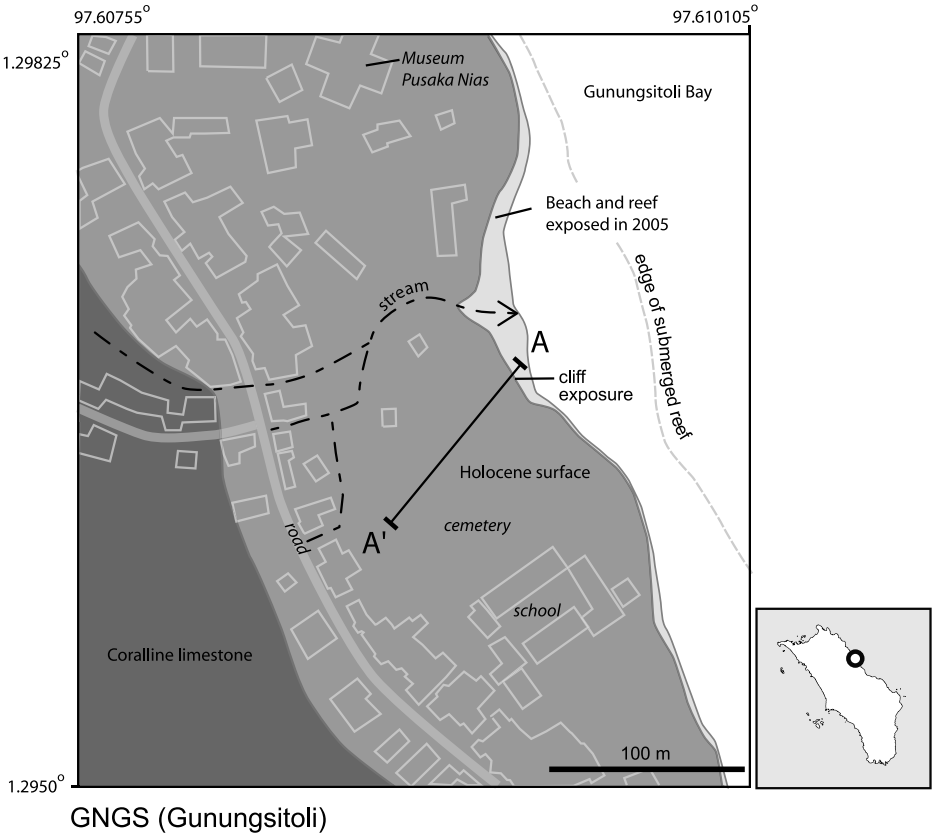

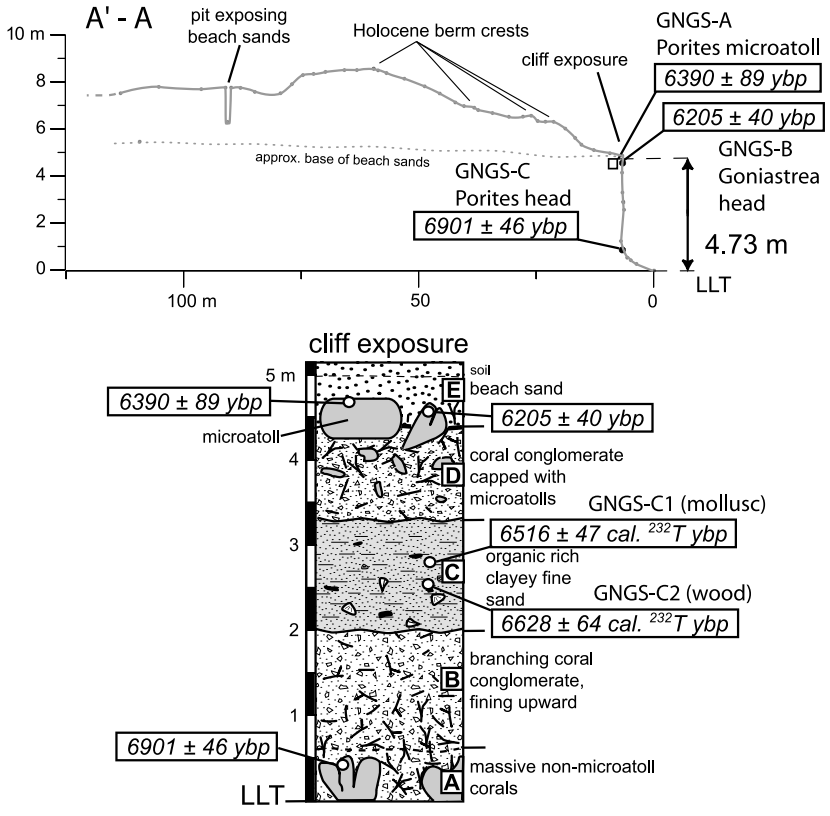

Figure 14. Surficial geologic map, topographic profile, and stratigraphic section at site GNGS.

Table 3. Radiocarbon Dates Reported in This Study

Lab ID[a]	Sample Name	Description	^{14}C Age ± 1σ[b]	δ^{13}C[c]	Marine Reservoir Correction[d]	Calibrated Years B.P. ± 1σ[e]	Calibrated ^{232}Th (years B.P.) ± 1σ[f]
CAMS 128784	RWB-LHWA-P1	mollusc	665 ± 30	0	441	255 ± 70	312 ± 70
CAMS 128785	RWB-LHWA-P2	peat	260 ± 35	−25	0	290 ± 135	347 ± 135
CAMS 128786	GN-1	marine gastropods	40,750 ± 540	0	441	44,996 ± 514	45,053 ± 514
AA 76022	RWB-LGND-C1	mollusc	4,474 ± 43	2.3	430	4,510 ± 68	4,567 ± 68
AA 76023	RWB-GLMB-C1	marine shell	postbomb	–	–	–	–
AA 76024	RWB-TETE-C1	marine shell	3,408 ± 37	3.0	430	3,161 ± 65	3,218 ± 65
AA 76025	RWB-GNGS-C1	mollusc	6,115 ± 42	−0.1	430	6,459 ± 47	6,516 ± 47
AA76021	RWB-GNGS-C2	woody debris	5,770 ± 41	−31.6	0	6,571 ± 64	6,628 ± 64
AA 76026	RWB-BAWZ-C1	gastropod	5,896 ± 42	1.1	430	6,270 ± 31	6,327 ± 31

[a]The ^{14}C AMS measurements performed at Center for Accelerator Mass Spectrometry (CAMS) at Lawrence Livermore National Laboratory and the NSF Arizona Accelerator Mass Spectrometry Laboratory (AA) at the University of Arizona.
[b]The quoted age is in radiocarbon years using the Libby half-life of 5568 years, relative to 1950 A.D.
[c]Values assumed according to *Stuiver and Polach* [1977] when given without decimal places.
[d]Marine reservoir correction from *Fairbanks et al.* [2005] for marine samples.
[e]Marine samples calibrated with Fairbanks et al. [2005] and terrestrial samples calibrated with Stuiver and Reimer [1993].
[f]To facilitate comparison with the 232Th dates reported for uplifted corals, this column adds 57 years (2007 – 1950) to each calibrated radiocarbon date.

obtained from a shallow well near the landward edge of the Holocene terrace.

[54] To determine net uplift at the site, we take the elevation of sample HILD-A (3.68 m), subtract the 2005 coseismic uplift (0.21 m) and apply the mid-Holocene sea level correction to obtain a net uplift value of 2.02 m. Dividing net uplift by the age of the head yields a tectonic uplift rate of 0.29 ± 0.15 mm/a.

[55] The ages of the dated heads here overlap the oldest dated sample at the next described site, Gunungsitoli, suggesting that the mid-Holocene sea level highstand on Nias was well under way by ~6900 years ago. Like site SIFI (Figure 12), the extensive flat surface does not appear to record sequential uplift by paleoearthquakes, but instead primarily reflects a long-lived mid-Holocene sea level highstand.

5.7. GNGS (Gunungsitoli)

[56] Much of the island's capital and main port city of Gunungsitoli is located on uplifted Holocene reefs, beaches, and alluvial deposits. In most places, human activities have substantially altered the original surfaces, but a rare pristine Holocene surface and cliff exposing Holocene reef and beach deposits is preserved at the GNGS site (Figures 2 and 14).

[57] A ~5-m cliff bounds the uplifted surface at GNGS on its seaward edge. Erosion of the sea cliff has exposed large (up to 2 m diameter) fossil coral heads. Massive nonmicroatoll *Porites* corals at the base of the exposure (unit A, Figure 14) are overlain by a fining upward breccia of branching corals and angular coral clasts (unit B). A distinctive dark colored unit of fine clayey sands with abundant organic material (unit C) sits conformably atop the basal coral breccia (unit D) along an even, sharp contact. Large in situ corals, including microatolls, are rooted in a coarse coral breccia that overlies the organic-rich layer. The entire exposure is covered by sand deposited in and among the large coral heads (unit E). The sand forms low (<1 m) berms on the surface.

[58] Age control for the exposure is provided by three U-Th dates on in situ coral heads and two radiocarbon dates obtained from organic material. A basal massive nonmicroatoll *Porites* head is 6901 ± 46 years old. A mollusc shell and woody debris from the muds of unit C are 6516 ± 47 and 6628 ± 64 cal ^{232}T years B.P., respectively (see Table 3 for an explanation of cal ^{232}T years B.P. ^{14}C dates). The uppermost head, a 1.5 m diameter *Porites* microatoll with a slightly eroded surface, is 6390 ± 89 years old, and a neighboring, slightly lower nonmicroatoll *Goniastrea* head is 6205 ± 40 years old.

[59] The stratigraphic sequence exposed in the sea cliff reflects a marine transgression (corals of unit A-D) and regression (beach sands of unit E and surface abandonment). The overall fining upward sequence in units A-C is consistent with the gradual infilling of a reef moat behind a more seaward reef crest [*Yamano et al.*, 2001]. The transition to coarser material at the contact between the muds of unit C and the coral rubble and reef rock of unit D can be interpreted in several ways. One possibility is that relative sea level fell temporarily but suddenly, perhaps due to tectonic uplift or nontectonic relative sea level fall, such that subaerial exposure of the reef crest caused coral rubble to be deposited into the reef moat during storms [*Scoffin*, 1993]. An equally plausible explanation is that the transition to coarse material at the unit C-D contact reflects lateral landward growth of the reef crest during a period of stable relative sea level [*Yamano et al.*, 2001]. In this scenario, landward expansion of the offshore reef crest during monotonic sea level rise or during a stable highstand led to deposition of coarse, storm-derived rubble into the margins of the moat region. Progressive shallowing of the moat eventually created a relatively calm, shallow zone in which the uppermost *Porites* microatolls in the cliff exposure could flourish. In either case, the 5 m exposure of reef corals records significant reef accretion over the interval between 7 and 6 ka, with subsequent deposition limited to minor aeolian remobilization of the uppermost beach sands.

[60] We calculate the net tectonic uplift rate at the site from the uppermost 6390 ± 90 year old *Porites* microatoll (4.73 m above LLT). With 2005 coseismic and Holocene RSL corrections are applied, the uplift rate is 0.49 ± 0.17 mm/a.

[61] It is worth noting that the terrace surface, which reaches more than 8 m above LLT, is considerably higher than the net tectonic uplift. This is due to the presence of an unusually thick mantle of beach sands, probably reworked from the nearby river. The depth of the overlying sands is nearly 3 m in places, as constrained by a pit along our

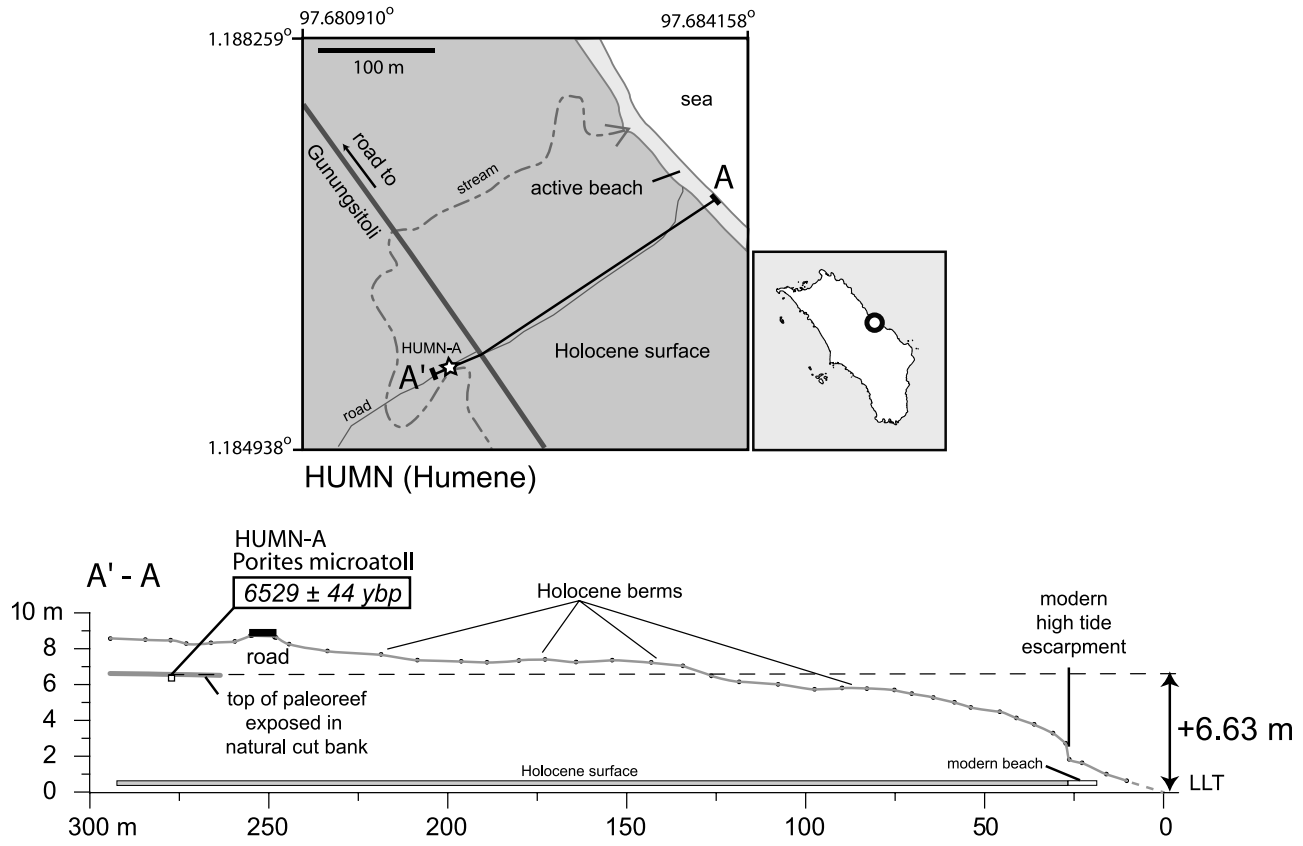

Figure 15. Surficial geologic map and topographic profile at site HUMN.

topographic transect and by exposures in the nearby stream banks.

5.8. HUMN (Desa Humene)

[62] A simple set of field relations at site HUMN (Figures 2 and 15) documents clear progressive uplift of a Holocene paleoreef. The site is located on the extensive, nearly continuous Holocene terrace that runs along much of the northeast coast of Nias. Transect A-A' crosses a sandy surface composed of broad recessional beach berms that climbs steadily to nearly 9 m over a distance of 300 m. Near the landward edge of the transect, a natural cut bank exposes a paleoreef topped by regressive beach sands. Landward of the paleoreef exposure, the surface flattens somewhat and continues ~250 m beyond the end of the transect until it laps onto a bedrock slope to the west; unfortunately, due to thick vegetation and restricted property access we could not extend our topographic profile to the shoreline angle. Even so, a *Porites* microatoll (HUMN-A) exposed in the cut bank 6.63 m above LLT yields a U-Th age of 6529 ± 44 years B.P.. When corrected for 0.24 m of 2005 coseismic uplift and 1.37 m of Holocene RSL change, the head yields an uplift rate of 0.77 ± 0.16 mm/a.

5.9. TDLU (Tedulehu)

[63] The Tedulehu study site (Figures 2 and 16) is on the narrow, continuous, elevated Holocene surface that runs along the southeast coast of Nias, in a zone that experienced ~0.25 m of coseismic subsidence in 2005. Long-term uplift at the site is clear: a well-defined terrace more than 4 m above LLT ornamented with numerous low beach berms extends from a small cliff backing the modern beach about 75 m inland, where it abuts a steep, completely recrystallized coralline limestone slope.

[64] We excavated a shallow (~1 m) pit at the back of the surface near the toe of a thin wedge of colluvium. The pit exposed several in situ nonmicroatoll *Goniastrea* heads rooted in cemented coral rubble and covered by beach sand (Figure 5d). The U-Th age we obtained on one of these heads, sample TDLU-B, is 6307 ± 45 years. Because the sampled head is not a microatoll, the elevation may underestimate paleo–low tide somewhat. However, the elevation of the head with respect to the rest of the surface and its proximity to the shoreline angle suggests that the head was growing within tens of centimeters of low tide when it died. The apparent elevation of sample TDLU-B is 4.0 m. We obtain a net uplift rate of 0.54 ± 0.15 mm/a after applying corrections for 2005 coseismic subsidence and mid-Holocene RSL variation.

5.10. LGND (Lagundri)

[65] Site LGND (Figures 2 and 17) is on the east side of Lagundri Bay, a popular surf destination on the southwest coast of Nias. Coseismic uplift in 2005 of 0.78 m resulted in intertidal exposure of a ~200 m wide reef and abrasion platform. The elevation transect here begins on the newly exposed platform and extends onto a low sandy Holocene surface before terminating at the landward edge on a sandstone bedrock slope. A pit in the Holocene surface did not expose unequivocally in situ coral heads. We sampled a large in situ *Porites* coral microatoll (LGND-A)

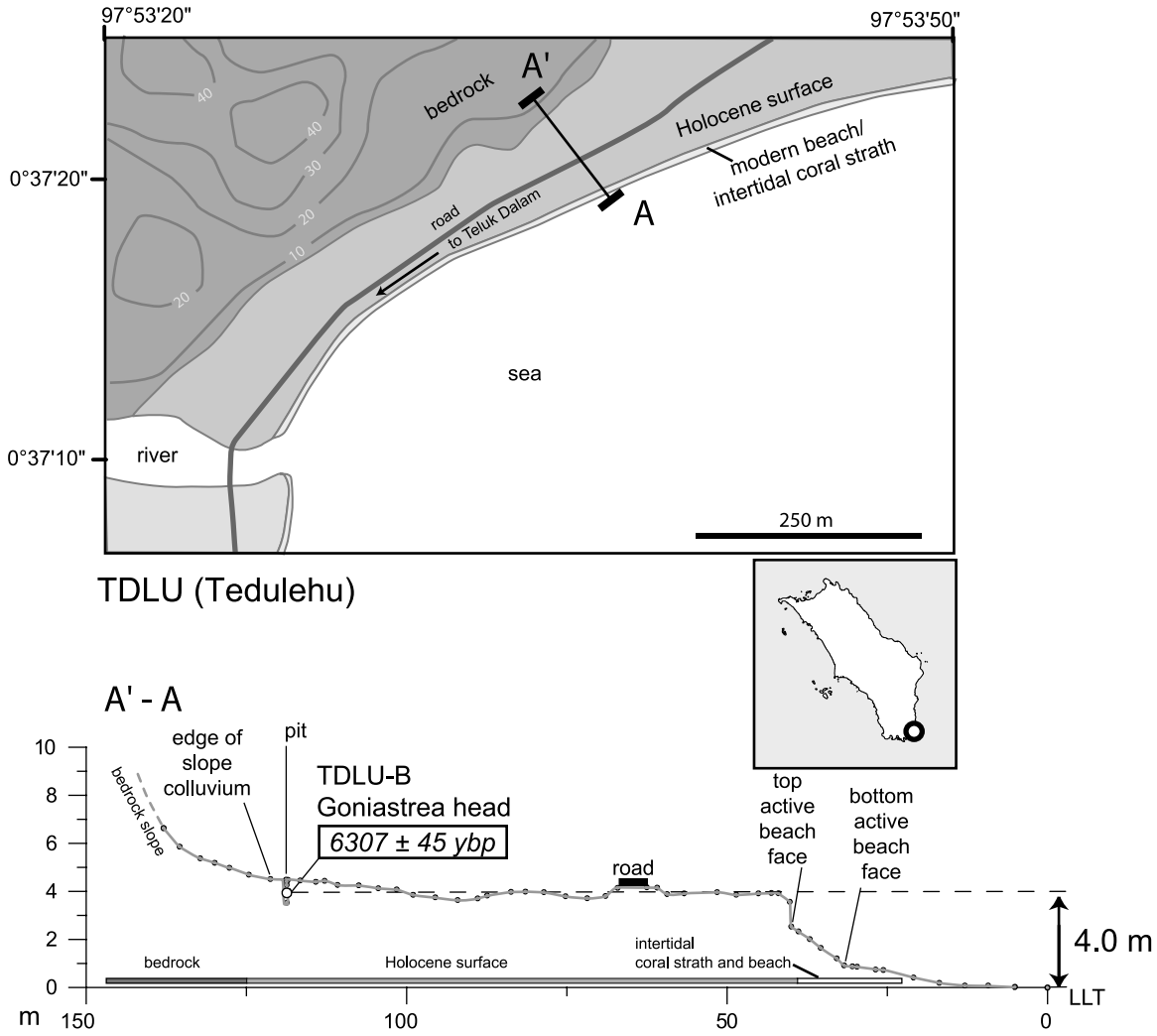

Figure 16. Surficial geologic map and topographic profile at site TDLU.

in a nearby freshly scoured canal overflow channel, which we project onto transect A-A'. The microatoll yielded a U-Th age of 5982 ± 60 years B.P., and is surprisingly low in elevation, only 0.59 m above LLT, such that prior to uplift in 2005, this head was lower than its modern counterparts. When corrected for Holocene RSL variation, the site yields a net subsidence rate of −0.19 ± 0.13 mm/a.

[66] In order to approximate the timing of beach berm emplacement atop the sampled microatoll, we obtained a ^{14}C date of 4570 ± 70 cal years B.P. from a mollusc shell incorporated in the base of the overlying berm. Given the several hundred meter paleoreef flat here and lack of scarps and elevation breaks in the Holocene surface, this date probably reflects the timing of beach progradation outward from the highstand shoreline during a relatively stable and sustained mid-Holocene highstand.

6. Discussion

6.1. Uplift Pattern

[67] The overall pattern of Holocene deformation on Nias is one of relatively low rates given the subduction zone context of our observations [e.g., *Ota and Yamaguchi*, 2004] and pronounced spatial variation (Figure 18 and Tables 1 and S1). Uplift rates are highest along the east coast, where maximum rates reach 1.5 mm/a (Figure 18). Lower uplift rates, and even net subsidence during the Holocene, occur along the remaining coastlines. In this section we explore the implications of the Holocene deformation pattern.

[68] Cross sections that juxtapose Holocene uplift rates with the 2005 coseismic uplift pattern (Figure 18) illustrate that Holocene deformation does not simply mirror 2005 coseismic uplift and subsidence. Rather, the pattern is nearly reversed: Holocene uplift rates are highest where coseismic uplift was nearly zero in 2005 and are substantially lower and even negative in locations where coseismic uplift of up to several meters occurred in 2005. Because the Holocene uplift rates and 2005 coseismic deformation patterns are clearly not correlated, the simple hypothesis that an increment of uplift due to megathrust slip in 2005 will be retained as permanent deformation of the island is not viable. Instead, the complex uplift and subsidence pattern strongly suggests that active deformation of the island occurs relatively slowly and heterogeneously along folds and faults in the hanging wall of the megathrust.

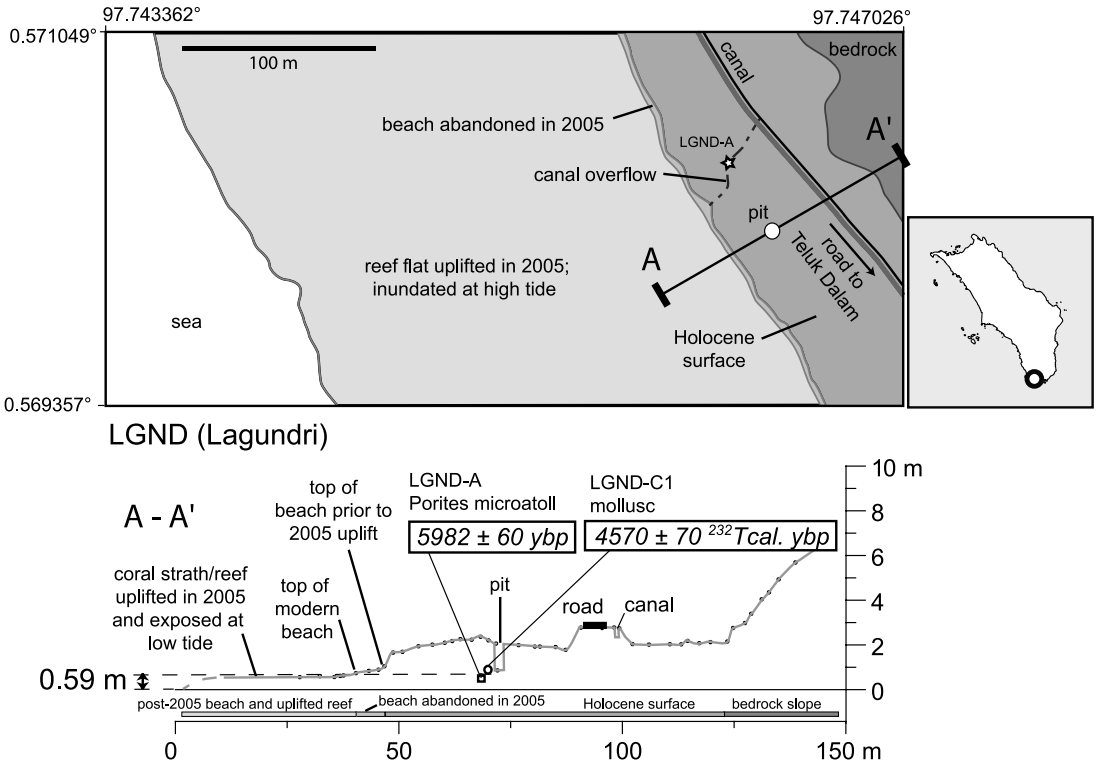

Figure 17. Surficial geologic map and topographic profile at site LGND.

[69] The pattern and rates of Holocene uplift and subsidence fall readily into three major domains of deformation (Figure 18). The first domain encompasses the highest elevated Holocene surfaces on Nias along the east coast, where surfaces as high as 11 m (e.g., site GLMB; Figures 2 and 10) slope steadily down to the sea and an extensive, uplifted Holocene coastal plain forms a prominent bulge in the eastern coastline. These surfaces reflect Holocene uplift rates as high as ~1.5 mm/a. The pronounced Holocene uplift preserved along the east coast is clearly not due to 2005-style coseismic deformation, because most of this coastline was stable or subsided slightly during the 2005 rupture. Instead, it is likely that the uplift along the east coast reflects motion on high-angle reverse faults in the upper plate (Figure 3) that form back thrusts with respect to the underlying decollement. A prominent flexural monocline along the east coast of Nias with over 3 km of structural relief was most active over the interval spanning the late Pliocene to early Pleistocene, and the flexure probably represents a buried, steeply west dipping thrust [*Karig et al.*, 1978; *Moore and Karig*, 1980]. Because recent uplift is occurring east of the flexure, we speculate that present-day deformation has stepped out to reverse faults that are seaward of the southeastern coast (Figure 3).

[70] Prominent tectonically uplifted Quaternary coral reefs on Nias are restricted to the northeast coast near Gunungsitoli [*Moore and Karig*, 1980; *Verstappen*, 1973]. These provide further evidence that recent deformation rates have been highest along the island's eastern margin (Figures 3 and 18). The Quaternary reefs near Gunungsitoli have been raised to ~130 m with an obvious lower bench at ~70 m. These reefs are nearly completely recrystallized and thus not easily dated, but if they grew during MIS 5e (120–130 ka) then their highest present positions would correspond to ~1 mm/a of uplift. This rate is twice as high as the Holocene rate we derive at Gunungsitoli (~0.5 mm/a) but comparable to the Holocene rates obtained along the southeast coast. It is equally plausible that the highest upraised reefs at Gunungsitoli are correlative with MIS 7 (230–270 ka), in which case the long-term rates of uplift equal the average rates of the past few thousand years. This latter interpretation would imply that the ~70 m reefs at Gunungsitoli are MIS 5e or 5c in age, despite their apparent recrystallization. Alternatively, if the MIS 5 reefs are indeed absent at Gunungsitoli, then an interval of substantial subsidence prior to recent uplift is required. Rapid uplift followed by equally rapid subsidence in an outer arc setting has been documented in the Solomon Islands and Vanuatu [*Taylor et al.*, 2005]. Detailed mapping and dating, if possible, of the older, elevated reefs on the east coast of Nias will be required to address this issue.

[71] Pronounced Holocene uplift along the east coast gives way to a zone of sustained stability or subsidence along the southern tip of the island, which is evident in (1) deep embayments that reflect drowning of the coast, (2) the low elevation of Holocene reefs (<3 m), and (3) the lack of upraised Quaternary reefs (Figure 3). We interpret the preservation of Holocene terraces here (e.g., site LGND) as due primarily to the mid-Holocene RSL high. Most of the southwestern coast between Lagundri and Sirombu lacks clear geomorphic or stratigraphic indicators of uplift. Instead, drainage patterns that flow inland and away from the coast and deep dendritic incision suggest a relict landscape that is retreating due to substantial coastal erosion. Existing seismic reflection profiles and bathymetry show large trench-slope basins adjacent to southeast Nias; these have

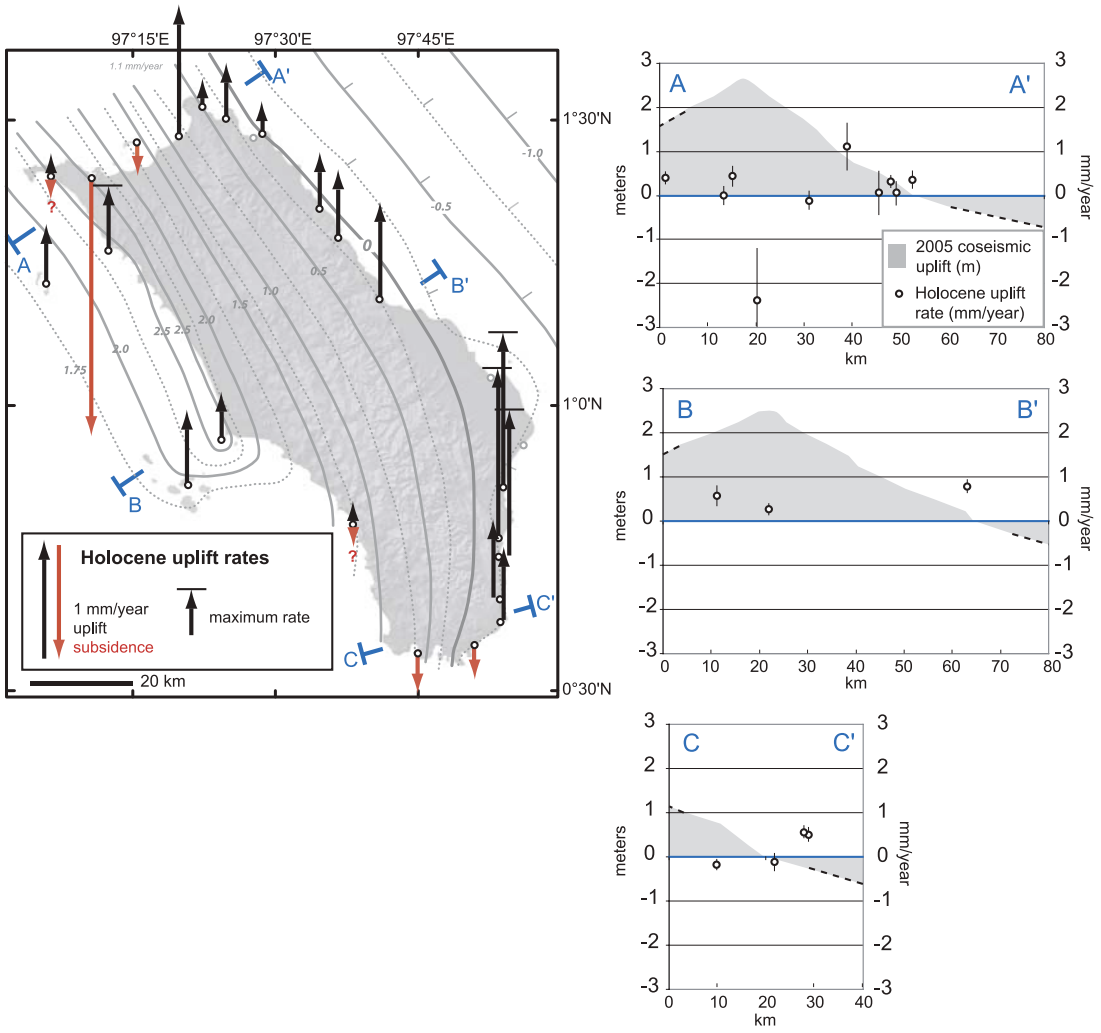

Figure 18. (left) Summary of Holocene uplift rates. Arrows are scaled to vertical rates. Arrows capped by bars signify maximum rates. Queried double-headed arrows represent sites that are nearly stable. (right) Comparison of the 2005 uplift pattern to Holocene uplift rates along three trench-perpendicular transects.

been interpreted as evidence of ongoing imbricate thrust faulting [*Moore and Curray*, 1980] but more detailed studies are required to test if these basins might actually reflect recent localized extension and trenchward collapse of the southwest coast of the island [*Milsom*, 2005].

[72] The northern and northwestern coasts, and their offshore islands, comprise the third and most varied zone of Holocene deformation on Nias. This zone experienced as much as 2.9 m of uplift due to megathrust slip in 2005, yet it is dominated by low rates of Holocene uplift, and some sites even exhibit subsidence. A series of closely spaced folded limestone terraces plunges into the sea along the northern coast (Figure 3), and the highly variable uplift rates in this zone, from −2.0 to 1.1 mm/a, reflect differential uplift, including pronounced local subsidence, along these structures. For example, rapid recent subsidence has occurred at site LHWA, consistent with its position in a small local synclinal trough and despite coseismic uplift of 2.47 m in 2005 (Figures 2 and 3). The general correlation of uplift rates with local structure is not perfect: site MZL has a relatively high uplift rate despite its location in a synclinal trough, which may reflect recent flexural slip in the syncline. Nonetheless, in general, the low deformation rates and their high spatial variability are consistent with deformation of the upper plate on local structures, rather than the influence of the megathrust strain accumulation and release cycle.

[73] Off the northwest coast, Wunga and the Hinako Islands define a geologically young ridge that is rising slightly faster than the mainland (Figures 3 and 18). This may represent deformation stepping trenchward from Nias [*Karig et al.*, 1978]. Curiously, this pattern does not continue to the south: The Hinako/Wunga ridge is truncated at a prominent geomorphic and structural divide at Sirombu (Figure 3), coincident with the beginning of the southward directed diminishment of 2005 megathrust slip (Figures 2 and 3). Furthermore, uplift of the eastern coastal plain suggests a change from trenchward (in the south) to landward dipping active fault vergence beneath Nias centered roughly on Sirombu (Figure 3). Bathymetric studies [*Ladage et al.*, 2006] show a clear reentrant in the trench beneath southern Nias, possibly controlled by impingement

of elevated bathymetry associated with the Wharton fossil ridge. It is tempting to speculate that the pronounced transition in structural styles across central Nias represents a structural boundary, possibly tied to structure or topography in the downgoing plate, that played a role in modulating slip during the 2005 rupture.

6.2. Elastic Versus Permanent Strain Along the Outer Arc High

[74] On the whole, Nias is rising at low rates considering its subduction zone setting, and portions of the island are even actively subsiding: uplift rates are no more than 1.5 mm/a and are generally $\leq$0.5 mm/a (Table 1 and Figure 18), with recent subsidence rates locally as high as 2 mm/a (site LHWA, Figure 11).

[75] These Holocene uplift rates are much lower than those reported in similar studies. For example, Middleton Island in Alaska occupies a structural position similar to Nias along the outer arc high and was uplifted 3.3 m during the great 1964 Alaskan megathrust rupture [*Plafker*, 1965; *Plafker and Rubin*, 1978]. A series of distinct elevated erosional platforms that fringe the island are most readily explained as shorelines abandoned due to sudden uplift during paleoearthquakes. These uplifted terraces record a Holocene uplift rate of $\sim$7–9 mm/a, which is inferred to occur along a blind thrust that splays upward from the underlying decollement [*Plafker and Rubin*, 1978]. Sequential coseismic uplift of the Boso Peninsula, Japan during historic megathrust ruptures has also been carefully documented [*Matsuda et al.*, 1978] and a Holocene uplift rate as high as $\sim$4 mm/a is evident from uplifted terraces [*Shimazaki and Nakata*, 1980]. The deformation pattern of elevated terraces on the peninsula is consistent with tilting due to faulting within the upper plate [*Scholz and Kato*, 1978] but may also reflect in part a local sharp bend in the plate boundary, persistent oblique slip on adjacent sections of the megathrust, or subduction of seamounts [*Stein et al.*, 2006; M. Shishikura et al., Fault model of the 1703 Genroku Kanto Earthquake (*M* 8.2) along the Sagami Trough deduced from renewed coseismic crustal deformation, unpublished manuscript, 2007]. Like Middleton Island, permanent uplift of the Boso Peninsula is probably due to intermittent motion on secondary structures or ramps rather than uncomplicated slip on the megathrust itself. Similar relationships of permanent deformation above megathrusts due to secondary faults and folds, and similarly high uplift rates in these settings, have been documented along subduction zones in New Zealand [*Berryman et al.*, 1989], the New Hebrides [*Taylor et al.*, 1990], the Solomon Islands [*Taylor et al.*, 2005], and Chile [*Melnick et al.*, 2006; *Nelson and Manley*, 1992].

[76] In contrast to the examples above, overall low elevations of uplifted Holocene reefs on Nias are evidence that strain accumulation and release in the hanging wall of the Sunda megathrust is nearly completely elastic at the millennial time scale and that upper plate faults and folds play a decidedly subordinate role in vertical deformation. This is consistent with qualitative observations (most outer arc highs are beneath sea level and thus are not subject to rapid vertical motions) but has not been quantified previously. Geodetic observations spanning a single megathrust earthquake cycle in Japan imply that interseismic deformation nearly cancels out coseismic deformation [*Thatcher*, 1984], but the link between these observations and longer time scales have only been inferred. A geologic long-term uplift rate of Nias of 0.2 mm/a has been calculated based on the time required to bring exposed lower Miocene strata to the surface from below the CCD [*Moore and Karig*, 1980]. Our observations of low Holocene uplift rates are consistent with this observation and imply that long-term and recent geological rates are similar in this setting.

[77] Seismic data and high-resolution bathymetry provide additional evidence for present-day tectonic stability of the Sunda outer-arc high. A series of multichannel and wide-angle seismic reflection profiles cross the fore arc adjacent to Java and southern Sumatra [*Kopp et al.*, 2002; *Kopp and Kukowski*, 2003; *Schlüter et al.*, 2002]. The reflection data, when coupled with refraction surveys [*Kopp et al.*, 2001], reveal pronounced net deformation and compaction of the material that forms the outer arc ridge, but little evidence of active deformation. Faults beneath the outer arc high are rotated out of active orientation and are crosscut by few, apparently slowly slipping out-of-sequence splay faults. The highly compacted, inactive region beneath the outer arc high is interpreted as a fossil accretionary wedge that now forms a relatively undeforming block against which more trenchward active deformation occurs. This interpretation is strengthened by bathymetric data that show a smooth surface above the nearly inactive outer arc high and a sharp increase in surface roughness in the trenchward direction above the active accretionary prism [*Kopp and Kukowski*, 2003].

[78] An important implication of our findings is that splay faulting and folding accompanying megathrust rupture plays a decidedly minor role in producing uplift on Nias, especially when viewed in the context of the broad, large amplitude elastic signal that accompanies megathrust rupture. To the north of Nias, high tsunami amplitudes and short arrival times along the Aceh coast following the 2004 M_w 9.2 Sumatra-Andaman rupture have led several investigators to speculate that rupture of an emergent splay accompanied megathrust rupture [*Plafker et al.*, 2006; *Sibuet et al.*, 2007]. However, tsunami arrival times along the Aceh coast may also be explained by simply extending slip more deeply along the megathrust in this region [*Chlieh et al.*, 2007; *Sladen and Hebert*, 2007], consistent with aftershock locations and focal mechanisms [*Dewey et al.*, 2007]. Our results suggest that emergent splays are the exception, rather than the rule, along the Sunda outer arc and that broad elastic uplift and subsidence signals are the dominant mode of megathrust coseismic outer arc deformation.

6.3. Coseismic Versus Interseismic Deformation

[79] When does slip occur on the upper plate faults and folds that slowly deform Nias? Slip on upper plate structures commonly accompanies megathrust earthquakes [*Clarke and Carver*, 1992; *Kelsey*, 1990; *McNeill et al.*, 1998]. However, we did not observe evidence for slip on secondary faults during the 2005 megathrust rupture, nor is intraplate deformation required to explain the dense coral and GPS geodetic measurements above the rupture patch [*Briggs et al.*, 2006; *Hsu et al.*, 2006]. This may be due to the resolution of our coral measurements and the coastal

bias of our observations, and it is possible that secondary faults or folds with up to a few tens of centimeters of displacement moved in 2005. However, we consider this possibility unlikely, as we have not observed emergent faults during post-2005 helicopter, road, and foot reconnaissance of the island, nor have any surface faults or belts of secondary deformation that might coincide with folds been reported by island residents or subsequent investigators.

[80] Sudden movement along upper plate faults might be expected to lead to sequences of progressively elevated and abandoned surfaces. Curiously, we do not observe such a simple and coherent paleoseismic record on Nias. Holocene surfaces along the north, south, and west coasts are remarkably broad and flat, with little evidence of tilting and an absence of sequentially uplifted and abandoned terraces. This is most simply explained as reflecting relative tectonic stability along these coasts, with terrace formation and preservation here due to the Holocene RSL highstand. On the east coast of Nias where recent uplift rates are highest, elevated Holocene surfaces generally slope gently to the sea without clear escarpments or sequentially abandoned surfaces that extend inland to the terrace edge. This raises the intriguing possibility that a significant portion of the deformation leading to permanent uplift of Nias occurs slowly and steadily in the interseismic period, rather than episodically due to brittle faulting in tandem with megathrust rupture. During the centuries between megathrust rupture, substantial elastic strain is stored in the upper plate, and this strain may lead to upper plate fault motion, either brittle or aseismic, or folding near the end of the subduction zone earthquake cycle. Aseismic slip along a blind thrust during the long interval between megathrust ruptures has been inferred beneath Isla Mocha Island off South America, where the elevations and widths of abandoned beach faces are suggestive of slow interseismic uplift [*Nelson and Manley*, 1992]. A similar mechanism may be at work in Alaska, where leveling data has been interpreted as showing continual motion of the splay fault beneath Middleton Island in the interseismic period [*Savage et al.*, 1998]. Interseismic deformation has also been invoked to explain net coastal uplift along the Cascadia subduction zone [*Kelsey et al.*, 1994], possibly due to deep postseismic slip on the megathrust following large ruptures [*Kelsey et al.*, 2006]. A full test of the hypothesis that Nias accumulates permanent deformation slowly and steadily during the interseismic interval will require a careful examination of chenier plain morphology and stratigraphy on the east coast and a close examination of future interseismic vertical geodetic signals.

6.4. Fraction of 2005 Coseismic Uplift Retained as Permanent Deformation

[81] One of our primary findings is that the fraction of 2005-type vertical displacements that will be retained as permanent uplift on Nias is generally very low or even nonexistent (that is, some long-term motions are opposite in sense from 2005 displacements). Furthermore, the retained fraction varies in regular fashion across Nias but does not match the 2005 uplift pattern, implying that processes other than retained deformation from 2005-type megathrust events are responsible for the Holocene uplift pattern.

[82] The 2005 and 1861 ruptures beneath Nias may not reflect a long-lived and stationary rupture patch (this remains to be tested by further paleoseismic data), but to the south of Nias in the Mentawai Islands region, the Sunda subduction zone appears to host ruptures that are remarkably consistent in their locations, if not in their slip per event [*Natawidjaja et al.*, 2007]. In many other subduction zones it is apparent that megathrust rupture patches may vary substantially in their locations, average slip amounts, and recurrence intervals (e.g., summary by *Satake and Atwater* [2007]). In this section, we explicitly compare the 2005 uplift pattern to longer-term (Holocene) vertical deformation. This provides the best available quantitative comparison between coseismic uplift and long-term deformation in the outer-arc setting. It is plausible that the 2005 and 1861 ruptures were not typical for this stretch of the subduction zone. If so, it still remains that the response of Nias to Holocene megathrust-induced uplift has been predominantly elastic, even if the slip distributions of previous megathrust ruptures have varied considerably.

[83] If we make the assumption that some fraction of permanent uplift from 2005-type megathrust ruptures will be retained as permanent deformation, we can place rough bounds on the inelastic or permanent component of uplift. This is illustrated in Table 4, which presents a rough calculation of the inelastic fraction that might be expected to be retained from 2005-type deformation. This calculation requires some knowledge of the recurrence interval for 2005-type events, which we assume ranges between 150 years (the approximate time between the 1861 and 2005 events) and 200 years (the approximate time required to accumulate the average slip beneath Nias in 2005 [see *Briggs et al.*, 2006]). We also assume that both 2005-type and long-term uplift accumulates steadily over the interval 0–7 ka. A comparison of the predicted long-term uplift as inferred from our coral measurements and the uplift that might be expected if 2005-type uplifts were entirely nonrecoverable allows us to calculate a retained fraction of uplift, expressed here as a percentage (Table 4).

[84] An interesting pattern emerges from this exercise: the sites that experienced the highest levels of uplift in 2005 can be expected to retain only a small fraction of that vertical deformation, while sites that subsided in 2005 are clearly rising in the long-term and thus the notion of a ''retained fraction'' does not easily apply to them. Table 4 presents the study sites ranked from positive (uplift) to negative (subsidence) vertical deformation in 2005. For sites that rose over 0.25 m in 2005, most will retain less than 0–4% of that uplift in the long-term. A slight exception is Hinako (HNKO), which might be expected to retain 5–7% of its 2005 uplift. This may reflect the position of Hinako above an inferred splay fault trenchward of Nias (although Wunga, above the same inferred structure, only retains 3–4% of 2005-type uplift). Some sites that experienced over 0.25 m of uplift in 2005, such as Senau (SEN) and Lagundri (LGND), appear to have subsided slightly during the Holocene.

[85] For sites that experienced less than 0.25 m of uplift in 2005, we infer retained fractions that range from 21 to 136%. These numbers must be viewed with caution, as their small uplift magnitudes, both in 2005 and in the long term, incorporate uncertainties nearly as large as the measure-

Table 4. Retained Fraction of 2005-Type Uplifts

Site[a]	2005 Coseismic Uplift[b] (m)	Cumulative Coseismic Uplift Since 7 ka[c] (m)	Long-Term Uplift Rate[d] (mm/a)	Cumulative Long-Term Uplift Since 7 ka[e] (m)	Retained Fraction of Total 2005-Type Uplift[f]
SRMB	2.56	119.5 to 89.6	0.26	1.84	~2%
HGWL	2.5	116.7 to 87.5	−0.02	−0.12	~0%
MBNA	2.34	109.2 to 81.9	0.47	3.27	3% to 4%
WNGA	1.81	84.5 to 63.4	0.38	2.67	3% to 4%
HNKO	1.75	81.7 to 61.3	0.63	4.40	5% to 7%
SEN	1.55	72.3 to 54.3	−0.14	−1.00	−1% to −2%
HMAZ	1.25	58.3 to 43.8	0.25	1.74	3% to 4%
LGND	0.78	36.4 to 27.3	−0.19	−1.31	−4% to −5%
SIFI	0.48	22.4 to 16.8	0.06	0.44	2% to 3%
GNGS	0.24	11.2 to 8.4	0.49	3.40	30% to 40%
HUMN	0.24	11.2 to 8.4	0.77	5.38	48% to 64%
HILD	0.21	9.8 to 7.4	0.29	2.06	21% to 28%
HILN	0.05	2.3 to 1.8	0.34	2.37	102% to 136%
LAYA	−0.1	−4.7 to −3.5	0.10	0.67	−14% to −19%
BAWZ	−0.25	−11.7 to −8.8	1.29	9.01	−77% to −103%
HLWA	−0.25	−11.7 to −8.8	0.55	3.83	−33% to −44%
TDLU	−0.25	−11.7 to −8.8	0.54	3.78	−32% to −43%
BAWF	−0.3	−14.0 to −10.5	0.30	2.07	−15% to −20%
GLMB	−0.3	−14.0 to −10.5	1.53	10.68	−76% to −102%
TETE	−0.3	−14.0 to −10.5	1.41	9.88	−71% to −94%

[a]Sites MZL and LHWA are excluded because the long-term uplift rate is calculated for an interval shorter than 2 ka.
[b]See Table 1.
[c]These values are obtained by assuming recurrence intervals of 150–200 years over the last 7 ka.
[d]See Table 1.
[e]These values are obtained by assuming a constant long-term uplift rate (see footnote c) for the last 7 ka. They closely approximate the actual net uplift of Holocene reefs and surfaces (see Table 1).
[f]Retained fraction is calculated by dividing the predicted long-term uplift since 7 ka (footnote e) by predicted coseismic uplift since 7 ka (footnote c).

ments themselves. It is most likely that these sites have been stable during the Holocene, but their small magnitudes of absolute vertical motion in 2005 and over the last 7 ka preclude careful analysis.

[86] Sites along the east coast of Nias that subsided in 2005 (negative coseismic uplift in Table 4) do not readily adhere to the notion of a "retained fraction," because their long-term net uplift rates are among the highest on the island despite their subsidence in 2005. We infer that a process distinct from megathrust rupture is responsible for the sustained uplift here. The responsible mechanism is unclear at present, but we hypothesize that steady uplift on a series of back thrusts along the eastern margin of the island during the interseismic interval is responsible for the observed uplifts. This hypothesis is supported by the steady coastward slopes of elevated surfaces and by the lack of sequentially abandoned surfaces along the east coast, as discussed above. Sites not located on the east coast are generally level and broad (e.g., SIFI, HILD) suggesting that these surfaces mostly record reef progradation during a relative sea level high and subsequent abandonment, rather than sequential tectonic uplift.

6.5. Holocene Relative Sea Level

[87] Because uplift rates on Nias are generally low with respect to other subduction zone settings [*Ota and Yamaguchi*, 2004], the poorly characterized Holocene RSL highstand of several meters on Nias adds considerable uncertainty to our uplift rate measurements (Table 1 and Figure 7). But considered in another light, the low overall rates of Holocene tectonic deformation provides for excellent geologic preservation of the Holocene highstand. Elevated microatolls and reef flat corals record the onset and duration of the relative sea level high, if not the amplitude. The highstand was well under way by 6.9 ka (e.g., sites HILD and SRMB) and probably began as early as 7.3 ka (site HILN). The landward edges of extensive, slightly elevated Holocene paleoreefs are dominated by heads that are generally 6–7 ka in age (Table 1). Sites that have been subject to very little Holocene deformation (e.g., SIFI) record a highstand that persisted until at least 2.0 ka with a maximum amplitude of only a few meters, as deduced from the level paleoreef and overlying recessional beach berms. A simple transgressive-regressive sequence of corals covered by beach deposits appears in sea cliff exposures (e.g., GNGS), and the seaward progression of younger coral ages on nearly level surfaces suggests progradation of the reef during a broad highstand that persisted over much of the mid- to late Holocene.

7. Summary and Tectonic Implications

[88] Low tectonic deformation rates and the dramatic mismatch between the long-term and 2005 uplift patterns on Nias strongly suggest that strain accumulation and release along the Sunda outer arc over dozens of megathrust earthquake cycles, that is, since the mid-Holocene, is nearly completely elastic. Sites that are subsiding or stable during the Holocene are clearly not retaining uplift from 2005-like events. Sites in the region of maximum 2005 uplift that are experiencing net uplift are rising so slowly that in general, less than 4% of the coseismic signal, assuming a 150- to 200-year return of 2005-style events, is being retained.

[89] We expect that future geologic investigations focusing on the active tectonics of other Sunda outer arc islands will confirm the picture of predominantly elastic strain accumulation and release that emerges from this study. The overall low relief and lack of clear young emergent terraces along the Mentawai Islands, the Batu Islands, and Simeulue hint that the entire length of the outer arc ridge is

dominated by the "yo-yo" motions (in the sense of *Plafker and Rubin* [1994]) that characterize Nias.

[90] Predominantly elastic behavior at the millennial time scale also suggests that elastic models are broadly appropriate for modeling the megathrust strain accumulation and release cycle along the Sunda megathrust. Given the morphologic similarity between Sunda and other accretionary subduction zones such as Cascadia, we expect that this finding extends to similar settings.

[91] We find that splay faulting has played only a subsidiary role in producing net vertical deformation over the course of the Holocene on Nias. This implies that broad elastic warps due to slip on the underlying megathrust, rather than discrete vertical displacements at the seafloor, characterize typical coseismic deformation along the Sunda outer arc high, a finding that has important implications for understanding tsunamigenesis along the Sunda subduction zone.

[92] A consequence of the dominance of elastic behavior on Nias is that most subduction zone earthquakes in this region do not leave a permanent record of uplifted geomorphic features. This is a corollary to a more familiar paleoseismic complication in subduction zone settings, which is that secondary faults and folds provide only a minimum estimate of megathrust earthquake recurrence [*Sieh*, 1981]. Considering the dominance of elastic behavior along the megathrust here, paleoearthquake studies in the Sunda region might best focus on sites that retain a stratigraphic record of cyclical strain accumulation and release, or on prograding surfaces like chenier plains that may record episodic uplift and subsidence (among other complex sedimentation processes) along their seaward edges. Also, the deaths of microatolls or paleoreef flats have been shown to provide reliable paleoearthquake information in the region [*Sieh et al.*, 1999; *Zachariasen et al.*, 1999]. This study highlights the fact that the Holocene record of vertical deformation in this region is not one of simple, sequential tectonic uplift.

[93] **Acknowledgments.** We thank the Captain and crew of the *Mentawai Indah*. Thanks to Hong-Wei Chiang and Larry Edwards for the U-Th dates. Dick Peltier and Rosemarie Drummond kindly provided predictions from the ICE-5G (VM2) model, and Aron Meltzner generously provided tide model calculations. We benefited greatly from discussions with Mike Gagan, Jean-Philippe Avouac, Glenn Milne, Chris Goldfinger, Harvey Kelsey, Ben Horton, and Heidrun Kopp. We also thank Daniel Melnick, Alan Nelson, two anonymous reviewers, and Associate Editor Greg Moore for their reviews and discussion of our manuscript. This work was supported by NSF (EAR-0610078) and a grant from the Gordon and Betty Moore Foundation. This is Caltech Tectonics Observatory contribution 80.

References

Adams, J. (1984), Active deformation of the Pacific Northwest continental margin, *Tectonics*, *3*, 449–472, doi:10.1029/TC003i004p00449.

Agnew, D. C. (1997), NLOADF: A program for computing ocean-tide loading, *J. Geophys. Res.*, *102*, 5109–5110, doi:10.1029/96JB03458.

Atwater, B. F. (1987), Evidence for great Holocene earthquakes along the outer coast of Washington State, *Science*, *236*, 942–944, doi:10.1126/science.236.4804.942.

Barber, A. J., and M. J. Crow (2005), Structure and structural history, in *Sumatra: Geology, Resources, and Tectonic Evolution*, edited by A. J. Barber et al., *Mem. Geol. Soc.*, *31*, 175–233.

Berryman, K. R., Y. Ota, and A. G. Hull (1989), Holocene paleoseismicity in the fold and thrust belt of the Hikurangi subduction zone, eastern North Island, New Zealand, *Tectonophysics*, *163*, 185–195, doi:10.1016/0040-1951(89)90256-4.

Bird, M. I., L. K. Fifield, T. S. Teh, C. H. Chang, N. Shirlaw, and K. Lambeck (2007), An inflection in the rate of early mid-Holocene eustatic sea-level rise: A new sea-level curve from Singapore, *Estuarine Coastal Shelf Sci.*, *71*, 523–536, doi:10.1016/j.ecss.2006.07.004.

Briggs, R. W., et al. (2006), Deformation and slip along the Sunda Megathrust in the great 2005 Nias-Simeulue earthquake, *Science*, *311*, 1897–1901, doi:10.1126/science.1122602.

Chappell, J. (1974), Geology of coral terraces, Huon Peninsula, New Guinea: A study of Quaternary tectonic movements and sea-level changes, *Geol. Soc. Am. Bull.*, *85*, 553–570, doi:10.1130/0016-7606(1974)85<553:GOCTHP>2.0.CO;2.

Cheng, H., R. L. Edwards, J. Hoff, C. D. Gallup, D. A. Richards, and Y. Asmerom (2000), The half-lives of uranium-234 and thorium-230, *Chem. Geol.*, *169*(1–2), 17–33, doi:10.1016/S0009-2541(99)00157-6.

Chlieh, M., et al. (2007), Coseismic slip and afterslip of the great M-w 9.15 Sumatra-Andaman earthquake of 2004, *Bull. Seismol. Soc. Am.*, *97*, S152–S173, doi:10.1785/0120050631.

Clark, J. A., W. E. Farrell, and W. R. Peltier (1978), Global Changes in Post-Glacial Sea-Level - Numerical-Calculation, *Quat. Res.*, *9*, 265–287, doi:10.1016/0033-5894(78)90033-9.

Clarke, S. H., and G. A. Carver (1992), Late Holocene tectonics and paleoseismicity, southern Cascadia Subduction Zone, *Science*, *255*, 188–192, doi:10.1126/science.255.5041.188.

Curray, J. R., and D. G. Moore (1974), Sedimentary and tectonic processes in the Bengal Deep-sea Fan and Geosyncline, in *Continental Margins*, edited by C. A. Burk and C. L. Drake, pp. 617–627, Springer, New York.

DeMets, C., R. G. Gordon, D. F. Argus, and S. Stein (1994), Effect of recent revisions to the geomagnetic reversal time-scale on estimates of current plate motions, *Geophys. Res. Lett.*, *21*, 2191–2194, doi:10.1029/94GL02118.

Dewey, J. W., G. Choy, B. Presgrave, S. Sipkin, A. C. Tarr, H. Benz, P. Earle, and D. Wald (2007), Seismicity associated with the Sumatra-Andaman Islands earthquake of 26 December 2004, *Bull. Seismol. Soc. Am.*, *97*, S25–S42, doi:10.1785/0120050626.

Diament, M., H. Harjono, K. Karta, C. Deplus, D. Dahrin, M. T. Zen Jr., M. Gérard, O. Lassal, A. Martin, and J. Malod (1992), Mentawai fault zone off Sumatra: A new key to the geodynamics of western Indonesia, *Geology*, *20*, 259–262, doi:10.1130/0091-7613(1992)020<0259:MFZOSA>2.3.CO;2.

Dickinson, W. R. (2001), Paleoshoreline record of relative Holocene sea levels on Pacific islands, *Earth Sci. Rev.*, *55*, 191–234, doi:10.1016/S0012-8252(01)00063-0.

Djamal, B., et al. (1991), *Laporan Geologi Lembar Nias*, Sumatera Geol. Res. and Dev. Cent., Bandung.

Edwards, R. L., J. H. Chen, and G. J. Wasserburg (1987), ^{238}U-^{234}U-^{230}Th-^{232}Th systematics and the precise measurement of time over the past 500,000 years, *Earth Planet. Sci. Lett.*, *81*, 175–192, doi:10.1016/0012-821X(87)90154-3.

Edwards, R. L., F. W. Taylor, and G. J. Wasserburg (1988), Dating earthquakes with high precision thorium-230 ages of very young corals, *Earth Planet. Sci. Lett.*, *90*, 371–381, doi:10.1016/0012-821X(88)90136-7.

Edwards, R. L., C. D. Gallup, and H. Cheng (2003), Uranium-series dating of marine and lacustrine carbonates, in *Uranium-Series Geochemistry, Rev. Mineral. Geochem*., vol. 52, edited B. Bourdon et al., pp. 363–405, Mineral. Soc. of Am., Washington, D. C.

Egbert, G. D., and S. Y. Erofeeva (2002), Efficient inverse modeling of barotropic ocean tides, *J. Atmos. Oceanic Technol.*, *19*, 183–204, doi:10.1175/1520-0426(2002)019<0183:EIMOBO>2.0.CO;2.

Fairbanks, R. G., et al. (2005), Radiocarbon calibration curve spanning 0 to 50,000 years BP based on paired $^{230}Th/^{234}U/^{238}U$ and ^{14}C dates on pristine corals, *Quat. Sci. Rev.*, *24*, 1781–1796, doi:10.1016/j.quascirev.2005.04.007.

Farr, T. G., et al. (2007), The Shuttle Radar Topography Mission, *Rev. Geophys.*, *45*, RG2004, doi:10.1029/2005RG000183.

Fitch, T. J., and C. H. Scholz (1971), Mechanism of underthrusting in southwest Japan: A model of convergent plate interactions, *J. Geophys. Res.*, *76*, 7260–7292, doi:10.1029/JB076i029p07260.

Geyh, M. A., H. Streif, and H.-R. Kudrass (1979), Sea-level changes during the late Pleistocene and Holocene in the Strait of Malacca, *Nature*, *278*, 441–443, doi:10.1038/278441a0.

Hamilton, W. (1979), Tectonics of the Indonesian region, *U.S. Geol. Surv. Prof. Pap.*, *1078*.

Horton, B. P., P. L. Gibbard, G. M. Mine, R. J. Morley, C. Purintavaragul, and J. M. Stargardt (2005), Holocene sea levels and palaeoenvironments, Malay-Thai Peninsula, southeast Asia, *Holocene*, *15*, 1199–1213, doi:10.1191/0959683605hl891rp.

Hsu, Y. J., et al. (2006), Frictional afterslip following the 2005 Nias-Simeulue earthquake, Sumatra, *Science*, *312*, 1921–1926, doi:10.1126/science.1126960.

Karig, D. E., et al. (1978), Structure and Cenozoic evolution of the Sunda arc in the central Sumatra region, in *Geological and Geophysical Inves-*

tigations of Continental Margins, edited by J. S. Watkins et al., *AAPG Mem. 29*, 223–237.

Kelsey, H. M. (1990), Late Quaternary deformation of marine terraces on the Cascadia Subduction Zone near Cape-Blanco, Oregon, *Tectonics*, *9*, 983–1014, doi:10.1029/TC009i005p00983.

Kelsey, H. M., D. C. Engebretson, C. E. Mitchell, and R. L. Ticknor (1994), Topographic form of the Coast Ranges of the Cascadia Margin in relation to coastal uplift rates and plate subduction, *J. Geophys. Res.*, *99*, 12,245–12,255, doi:10.1029/93JB03236.

Kelsey, H., K. Satake, Y. Sawai, B. Sherrod, K. Shimokawa, and M. Shishikura (2006), Recurrence of postseismic coastal uplift, Kuril subduction zone, Japan, *Geophys. Res. Lett.*, *33*, L13315, doi:10.1029/2006GL026052.

Konca, A. O., et al. (2007), Rupture kinematics of the 2005 M-w 8.6 Nias-Simeulue earthquake from the joint inversion of seismic and geodetic data, *Bull. Seismol. Soc. Am.*, *97*, S307–S322, doi:10.1785/0120050632.

Kopp, H., and N. Kukowski (2003), Backstop geometry and accretionary mechanics of the Sunda margin, *Tectonics*, *22*(6), 1072, doi:10.1029/2002TC001420.

Kopp, H., E. R. Flueh, D. Klaeschen, J. Bialas, and C. Reichert (2001), Crustal structure of the central Sunda margin at the onset of oblique subduction, *Geophys. J. Int.*, *147*, 449–474, doi:10.1046/j.0956-540x.2001.01547.x.

Kopp, H., D. Klaeschen, E. R. Flueh, J. Bialas, and C. Reichert (2002), Crustal structure of the Java margin from seismic wide-angle and multichannel reflection data, *J. Geophys. Res.*, *107*(B2), 2034, doi:10.1029/2000JB000095.

Ladage, S., et al. (2006), Bathymetric survey images structure off Sumatra, *Eos Trans. AGU*, *87*, 165.

Matsuda, T., Y. Ot, M. Ando, and N. Yonekura (1978), Fault mechanism and recurrence time of major earthquakes in southern Kanto district, Japan, as deduced from coastal terrace data, *Geol. Soc. Am. Bull.*, *89*, 1610–1618, doi:10.1130/0016-7606(1978)89<1610:FMARTO>2.0.CO;2.

McNeill, L., C. Goldfinger, R. S. Yeats, and L. D. Kulm (1998), The effects of upper plate deformation on records of prehistoric Cascadia subduction zone earthquakes, in *Coastal Tectonics*, edited by I. S. Stewart and C. Vita-Finzi, *Geol. Soc. Spec. Publ.*, *146*, 321–342.

Melnick, D., B. Bookhagen, H. P. Echtler, and M. R. Strecker (2006), Coastal deformation and great subduction earthquakes, Isla Santa Maria, Chile (37°S), *Geol. Soc. Am. Bull.*, *118*, 1463–1480, doi:10.1130/B25865.1.

Meltzner, A. J., K. Sieh, M. Abrams, D. C. Agnew, K. W. Hudnut, J.-P. Avouac, and D. H. Natawidjaja (2006), Uplift and subsidence associated with the great Aceh-Andaman earthquake of 2004, *J. Geophys. Res.*, *111*, B02407, doi:10.1029/2005JB003891.

Milsom, J. S. (2005), Seismology and neotectonics, in *Sumatra: Geology, Resources, and Tectonic Evolution*, edited by A. J. Barber et al., *Mem. Geol. Soc.*, *31*, 7–15.

Mitrovica, J. X., and G. M. Milne (2002), On the origin of late Holocene sea-level highstands within equatorial ocean basins, *Quat. Sci. Rev.*, *21*, 2179–2190, doi:10.1016/S0277-3791(02)00080-X.

Moore, G. F., and J. R. Curray (1980), Structure of the Sunda Trench lower slope off Sumatra from multichannel seismic reflection data, *Mar. Geophys. Res.*, *4*, 319–340, doi:10.1007/BF00369106.

Moore, G. F., and D. E. Karig (1980), Structural geology of Nias Island, Indonesia; implications for subduction zone tectonics, *Am. J. Sci.*, *280*, 193–223.

Moore, G. F., et al. (1982), Sedimentation in the Sunda Trench and forearc region, in *Trench-Forearc Geology: Sedimentation and Tectonics on Modern and Ancient Active Plate Margins*, edited by J. K. Leggett, *Geol. Soc. Spec. Publ.*, *10*, 245–258.

Natawidjaja, D., et al. (2007), A 700-year paleoseismic context for the Sumatran megathrust earthquakes of 2007, *Eos Trans. AGU*, *88*(52), Fall Meet. Suppl., Abstract U53A-01.

Nelson, A. R., and W. F. Manley (1992), Holocene coseismic and aseismic uplift of Isla Mocha, south-central Chile, *Quaternary Int.*, *15–16*, 61–76, doi:10.1016/1040-6182(92)90036-2.

Newcomb, K., and W. McCann (1987), Seismic history and seismotectonics of the Sunda arc, *J. Geophys. Res.*, *92*, 421–439, doi:10.1029/JB092iB01p00421.

Ota, Y., and M. Yamaguchi (2004), Holocene coastal uplift in the western Pacific Rim in the context of late Quaternary uplift, *Quat. Int.*, *120*, 105–117, doi:10.1016/j.quaint.2004.01.010.

Peltier, W. R. (2004), Global glacial isostasy and the surface of the ice-age earth: The ice-5G (VM2) model and grace, *Annu. Rev. Earth Planet. Sci.*, *32*, 111–149, doi:10.1146/annurev.earth.32.082503.144359.

Plafker, G. (1965), Tectonic deformation associated with 1964 Alaska earthquake—Earthquake of 27 March 1964 resulted in observable crustal deformation of unprecedented areal extent, *Science*, *148*, 1675–1687, doi:10.1126/science.148.3678.1675.

Plafker, G., and M. Rubin (1978), Uplift history and earthquake recurrence as deduced from marine terraces on Middleton Island, Alaska, *U.S. Geol. Surv. Open File Rep.*, *78-943*, 687–721.

Plafker, G., and M. Rubin (1994), Paleoseismic evidence for ''yo-yo'' tectonics above the eastern Aleutian subduction zone: Coseismic uplift alternating with even larger interseismic submergence, in *Proceedings of the Workshop on Paleoseismology*, convened by C. S. Prentice, D. P. Schwartz, and R. S. Yeats, *U. S. Geol. Surv. Open File Rep., 94-568*, 155–157.

Plafker, G., and J. C. Savage (1970), Mechanism of the Chilean earthquakes of May 21 and 22, 1960, *Geol. Soc. Am. Bull.*, *81*, 1001–1030, doi:10.1130/0016-7606(1970)81[1001:MOTCEO]2.0.CO;2.

Plafker, G., et al. (2006), The cataclysmic 2004 tsunami on NW Sumatra - Preliminary evidence for a near-field secondary source along the Western Aceh Basin, paper presented at Annual Meeting, Seismol. Soc. of Am., San Francisco, Calif.

Prawirodirdjo, L., and Y. Bock (2004), Instantaneous global plate motion model from 12 years of continuous GPS observations, *J. Geophys. Res.*, *109*, B08405, doi:10.1029/2003JB002944.

Samuel, M., and N. Harbury (1996), The Mentawai fault zone and deformation of the Sumatran forearc in the Nias area, in *Tectonic Evolution of Southeast Asia*, edited by R. Hall and D. Blundell, *Geol. Soc. Spec. Publ.*, *106*, 337–351.

Samuel, M. A., N. A. Harbury, A. Bakria, F. T. Banner, and L. Hartono (1997), A new stratigraphy for the islands of the Sumatran forearc, Indonesia, *J. Asian Earth Sci.*, *15*, 339, doi:10.1016/S0743-9547(97)87720-3.

Satake, K., and B. F. Atwater (2007), Long-term perspectives on giant earthquakes and tsunamies at subduction zones, *Annu. Rev. Earth Planet. Sci.*, *35*, 349–374, doi:10.1146/annurev.earth.35.031306.140302.

Savage, J. C. (1983), A dislocation model of strain accumulation and release at a subduction zone, *J. Geophys. Res.*, *88*, 4984–4996, doi:10.1029/JB088iB06p04984.

Savage, J. C., J. L. Svarc, W. H. Prescott, and W. K. Gross (1998), Deformation across the rupture zone of the 1964 Alaska earthquake, 1993–1997, *J. Geophys. Res.*, *103*(B9), 21,275–21,283, doi:10.1029/98JB02048.

Schlüter, H. U., C. Gaedicke, H. A. Roeser, B. Schreckenberger, H. Meyer, C. Reichert, Y. Djajadihardja, and A. Prexl (2002), Tectonic features of the southern Sumatra-western Java forearc of Indonesia, *Tectonics*, *21*(5), 1047, doi:10.1029/2001TC901048.

Scholz, C. H., and T. Kato (1978), The behavior of a convergent plate boundary: Crustal deformation in the South Kanto district, Japan, *J. Geophys. Res.*, *83*, 783–797, doi:10.1029/JB083iB02p00783.

Scoffin, T. P. (1993), The geological effects of hurricanes on coral-reefs and the interpretation of storm deposits, *Coral Reefs*, *12*, 203–221, doi:10.1007/BF00334480.

Scoffin, T. P., and M. D. A. Le Tissier (1998), Late Holocene sea level and reef flat progradation, Phuket, South Thailand, *Coral Reefs*, *17*, 273–276, doi:10.1007/s003380050128.

Scoffin, T. P., and D. R. Stoddart (1978), The nature and significance of microatolls, *Philos. Trans. R. Soc. London, Ser. B*, *284*, 99–122, doi:10.1098/rstb.1978.0055.

Shimazaki, K., and T. Nakata (1980), Time-predictable recurrence model for large earthquakes, *Geophys. Res. Lett.*, *7*, 279–282, doi:10.1029/GL007i004p00279.

Sibuet, J. C., et al. (2007), 26th December 2004 great Sumatra-Andaman earthquake: Co-seismic and post-seismic motions in northern Sumatra, *Earth Planet. Sci. Lett.*, *263*, 88–103, doi:10.1016/j.epsl.2007.09.005.

Sieh, K. (1981), A review of geological evidence for recurrence times of large earthquakes, in *Earthquake Prediction: An International Review, Maurice Ewing Ser.*, vol. 4, edited W. Simpson and P. G. Richards, pp. 181–207, AGU, Washington, D. C.

Sieh, K., and D. Natawidjaja (2000), Neotectonics of the Sumatran fault, Indonesia, *J. Geophys. Res.*, *105*, 28,295–28,326, doi:10.1029/2000JB900120.

Sieh, K., S. N. Ward, D. Natawidjaja, and B. W. Suwargadi (1999), Crustal deformation at the Sumatran subduction zone revealed by coral rings, *Geophys. Res. Lett.*, *26*(20), 3141–3144, doi:10.1029/1999GL005409.

Sladen, A., and H. Hebert (2007), On the use of satellite altimetry to infer the earthquake rupture characteristics: Application to the 2004 Sumatra event, *Geophys. J. Int.*, *172*, 707–714, doi:10.1111/j.1365-246X.2007.03669.x.

Smith, W. H. F., and D. T. Sandwell (1997), Global sea floor topography from satellite altimetry and ship depth soundings, *Science*, *277*, 1956–1962, doi:10.1126/science.277.5334.1956.

Smithers, S. G., and C. D. Woodroffe (2000), Microatolls as sea-level indicators on a mid-ocean atoll, *Mar. Geol.*, *168*, 61–78, doi:10.1016/S0025-3227(00)00043-8.

Stein, R. S., S. Toda, T. Parsons, and E. Grunewald (2006), A new probabilistic seismic hazard assessment for greater Tokyo, *Philos. Trans. R. Soc. London, Ser. A*, *364*, 1965–1986, doi:10.1098/rsta.2006.1808.

Stuiver, M., and H. A. Polach (1977), Discussion: Reporting of ^{14}C data, *Radiocarbon*, *19*, 355–363.

Stuiver, M., and P. J. Reimer (1993), Extended ^{14}C database and revised CALIB radiocarbon calibration program, *Radiocarbon*, *35*, 215–230.

Stuiver, M., et al. (1998), INTCAL98 radiocarbon age calibration, 24,000–0 cal BP, *Radiocarbon*, *40*, 1041–1083.

Taylor, F. W., B. L. Isacks, C. Jouannic, A. L. Bloom, and J. Dubois (1980), Coseismic and Quaternary vertical tectonic movements, Santo and Malekula islands, New Hebrides Island Arc, *J. Geophys. Res.*, *85*, 5367–5381, doi:10.1029/JB085iB10p05367.

Taylor, F. W., C. Frohlich, J. Lecolle, and M. Strecker (1987), Analysis of partially emerged corals and reef terraces in the central Vanuatu Arc: Comparison of contemporary coseismic and nonseismic with Quaternary vertical movements, *J. Geophys. Res.*, *92*, 4905–4933, doi:10.1029/JB092iB06p04905.

Taylor, F. W., R. L. Edwards, G. J. Wasserburg, and C. Frohlich (1990), Seismic recurrence intervals and timing of aseismic subduction inferred from emerged corals and reefs of the central Vanuatu (New Hebrides) frontal arc, *J. Geophys. Res.*, *95*, 393–408, doi:10.1029/JB095iB01p00393.

Taylor, F. W., et al. (2005), Rapid forearc uplift and subsidence caused by impinging bathymetric features: Examples from the New Hebrides and Solomon arcs, *Tectonics*, *24*, TC6005, doi:10.1029/2004TC001650.

Thatcher, W. (1984), The earthquake deformation cycle at the Nankai Trough, southwest Japan, *J. Geophys. Res.*, *89*, 3087–3101, doi:10.1029/JB089iB05p03087.

Tjia, H. D. (1996), Sea-level changes in the tectonically stable Malay-Thai Peninsula, *Quaternary Int.*, *31*, 95–101, doi:10.1016/1040-6182(95)00025-E.

Verstappen, H. T. (1973), *A Geomorphological Reconnaissance of Sumatra and Adjacent Islands*, Wolters-Noordhof, Groningen, Netherlands.

Vita-Finzi, C. (1995), Pulses of emergence in the outer-arc ridge of the Sunda arc, *J. Coastal Res.*, *17*(spec. issue), 279–281.

Vita-Finzi, C., and B. Situmorang (1989), Holocene coastal deformation in Simeulue and Nias, Indonesia, *Mar. Geol.*, *89*, 153–161, doi:10.1016/0025-3227(89)90031-5.

Wang, K., R. Wells, S. Mazzotti, R. D. Hyndman, and T. Sagiya (2003), A revised dislocation model of interseismic deformation of the Cascadia subduction zone, *J. Geophys. Res.*, *108*(B1), 2026, doi:10.1029/2001JB001227.

Whittaker, J. M., et al. (2007), Sunda-Java trench kinematics, slab window formation and overriding plate deformation since the Cretaceous, *Earth Planet. Sci. Lett.*, *255*, 445–457, doi:10.1016/j.epsl.2006.12.031.

Yamano, H., et al. (2001), Coral reef evolution at the leeward side of Ishigaki Island, southwest Japan, *Radiocarbon*, *43*, 899–908.

Zachariasen, J. (1998), Paleoseismology and paleogeodesy of the Sumatran subduction zone: A study of vertical deformation using coral microatolls, Ph.D. dissertation thesis, Calif. Inst. of Technol., Pasadena.

Zachariasen, J., K. Sieh, F. W. Taylor, R. L. Edwards, and W. S. Hantoro (1999), Submergence and uplift associated with the giant 1833 Sumatran subduction earthquake: Evidence from coral microatolls, *J. Geophys. Res.*, *104*, 895–919, doi:10.1029/1998JB900050.

W. H. Amidon and J. Galetzka, Tectonics Observatory, Division of Geological and Planetary Sciences, California Institute of Technology, MC 100-23, Pasadena, CA 91125, USA.

R. W. Briggs, Geologic Hazards Team, U.S. Geological Survey, MS 966, Box 25046, Golden, CO 80225, USA. (rbriggs@usgs.gov)

T. G. Farr, Jet Propulsion Laboratory, California Institute of Technology, M/S 300-233, 4800 Oak Grove Drive, Pasadena, CA 91125, USA.

D. Natawidjaja, D. Prayudi, N. Sastra, and B. Suwargadi, Research Center for Geotechnology, Indonesian Institute of Sciences, Bandung, Indonesia 40135.

I. Suprihanto, Jalan Mahoni, Blok E, Gang I., No 13, Route 002/015, Kota Jakarta 14270, Indonesia.

K. Sieh, Earth Observatory of Singapore, Nanyang Technological University, 70 Nanyang Drive, Block N1.3, Level B1, Singapore 637457.